Geomech. Geophys. Geo-energ. Geo-resour. (2021) 7:71
https://doi.org/10.1007/s40948-021-00262-5

ORIGINAL ARTICLE

Pore structure and sorption capacity investigations of Ediacaran and Lower Silurian gas shales from the Upper Yangtze platform, China

Zhazha Hu · Garri Gaus · Timo Seemann · Qian Zhang · Ralf Littke · Reinhard Fink

Received: 19 August 2020 / Accepted: 21 May 2021 / Published online: 16 June 2021

Abstract The shale gas potential of Ediacaran and Lower Silurian shales from the Upper Yangtze platform is assessed in this study with a focus on the contributions of clay minerals and organic matter to sorption capacity. For this purpose, a multidisciplinary assessment was carried out using petrophysical, mineralogical, petrographic and geochemical methods. In terms of TOC contents (4.2%), brittle mineral contents (68.6%) and maximum gas storage capacities (0.054–0.251 mmol/g) Ediacaran shales from this study show comparable properties to other producing shale gas systems although the thermal maturity is extremely high (VR_r = 3.6%). When compared to lower Silurian shales from the same region, it is evident that (1) deeper maximum burial and (2) a lack of silica-associated preservation of the pores resulted in a relatively lower mesopore volume, higher micropore volume fraction and lower overall porosity (Ediacaran shales: 1.4–4.6%; Silurian shales: 6.2–7.4%). Gas production is therefore retarded by poor interconnectivity of the pore system, which was qualitatively demonstrated by comparing experimental gas uptake kinetics. TOC content exhibits a prominent control on sorption capacity and micropore volume for both shales. However, different contributions of clay minerals to sorption capacity were identified. This can partly be attributed to different clay types but is likely also related to burial-induced recrystallisation and different origins of illite. Additionally, it was shown that variations in sorption capacity due to incorrect estimates of clay mineral contribution are in the same range as variations due to differences in thermal maturity.

Article highlights

- Pore structure and gas storage characteristics are evaluated for the first time for Ediacaran Shales from the Upper Yangtze platform
- Due to a lower free gas storage capacity and diffusivity, the Ediacaran shale can be regarded as a less favorable shale gas prospect when compared to the Silurian shale
- Clay mineral contribution to sorption capacity is evaluated taking clay mineralogy into consideration
- Maturity-related changes of organic matter sorption capacity have been discussed on the basis of a compiled data set

Keywords Ediacaran · Silurian · Sorption capacity · Pore structure · Mineralogy · Thermal maturity

Z. Hu · G. Gaus (✉) · Q. Zhang · R. Littke · R. Fink
Institute of Geology and Geochemistry of Petroleum and Coal, Energy and Mineral Resources Group (EMR), RWTH Aachen University, Lochnerstr. 4-20, 52062 Aachen, Germany
e-mail: garri.gaus@emr.rwth-aachen.de

T. Seemann
Institute of Clay and Interface Mineralogy, Energy and Mineral Resources Group (EMR), RWTH Aachen University, Bunsenstraße 8, 52072 Aachen, Germany

1 Introduction

Shale gas production in China progressed fast from 0.025 billion cubic meter (bcm) in 2012 to 10.88 bcm in 2018 but is still in an initial stage when compared to the United States (624.40 bcm in 2018) (Zhai et al. 2018; Wang et al. 2019; Dai et al. 2020). Therefore, the identification of additional shale gas prospects is currently prioritized in China (Nie et al. 2009; Han et al. 2013; Zou et al. 2014; Dang et al. 2016; Li et al. 2020). With respect to the economic potential of shale gas reservoirs, an accurate estimation of the maximum amount of gas stored (Gas in Place, GIP) is essential. Hence, investigations of gas storage estimates (porosity, excess sorption capacity) and their controlling properties (TOC content, clay content, moisture, thermal maturity, micropore volume, and accessibility) are of major interest.

To date, major commercial shale gas production in China is limited to the Upper Ordovician Wufeng and Lower Silurian Longmaxi formations with an annual production of approximately 6 bcm in the Fuling gas field in 2017 (Chen et al. 2018). Additionally, a series of test wells were drilled on over-mature Cambrian and Ediacaran shales in the western Hubei province. The "Eyiye-1" test well, targeting the Cambrian Shuijingtuo formation, produced 6.02×10^4 m^3 gas per day in May 2017 (Chen et al. 2018). Retrieved cores from test wells "Zidi 1" and "Zidi 2" targeting the Ediacaran Doushantuo formation revealed a total gas content of 0.337–1.666 m^3/t (0.015–0.073 mmol/g) at IUPAC standard conditions (273.15 K and 10^5 Pa) from canister desorption experiments on site (Li et al. 2019). Additionally, for the horizontally drilled "Eyangye-2HF" well, a gas production rate of up to 5.53×10^4 m^3/day was achieved from the Ediacaran Doushantuo formation in 2018 (Wang et al. 2019). When compared to the average gas production rate (12.87×10^4 m^3/day) and total gas content (1.9–8.0 m^3/t or 0.083–0.352 mmol/g at IUPAC conditions) of the Wufeng and Longmaxi shale formations (Zou et al. 2014, 2016), these test wells indicate good exploitation potential of Proterozoic shales in the Yangtze platform. Therefore, an appraisal of the economic potential of Ediacaran shale gas reservoirs is of particular importance. While numerous studies were performed to characterize storage properties of the Wufeng-Longmaxi shales (Yang et al. 2015, 2016, 2017; Wang et al. 2016), only a few studies thus far focused on shales from the Ediacaran (Chen et al. 2016; Yang et al. 2020). These shales, though extremely high in thermal maturity (approximately 4.0% in equivalent vitrinite reflectance), are rich in organic matter (TOC content of up to 8.0 wt.%) and widely distributed in the area of the Upper Yangtze platform with thicknesses of 200 to 900 m. The well-studied Silurian Longmaxi Shale in the Sichuan Basin has a lower thermal maturity (2.0–3.2%), smaller thickness from 100 to 500 m, exhibits high TOC contents (up to 8.3 wt.%) as well as porosity (3.4–8.2%) (Zou et al. 2014; Yang et al. 2015; Zhang et al. 2019).

Natural gas in shales can be stored in the free, dissolved and adsorbed state (Gasparik et al. 2014; Clarkson et al. 2016). Free gas is stored volumetrically in both pore and fracture space, whereas dissolved gas is the proportion of gas dissolved in formation water, liquid hydrocarbon or absorbed by solid kerogen (Zhang et al. 2012). The enrichment of gas on the surface of organic matter or minerals is referred to as adsorbed gas (Hildenbrand et al. 2006). In this study, the term "sorption" covers any state of gas storage except for the free state because a differentiation between adsorption and dissolution is currently not possible in the laboratory.

Several studies imply that gas stored in the sorbed phase can contribute up to 60% of the total gas storage capacity of shales (Lu et al. 1995; Rexer et al. 2013). Sorption capacity can therefore not be neglected in the evaluation of GIP estimations. In this context, isothermal high-pressure methane sorption experiments are widely applied to assess the maximum sorption capacity of shales (Gensterblum et al. 2009; Rexer et al. 2013). Major controls on methane sorption capacity were identified as organic matter content and type, thermal maturity, clay mineral content and type, moisture, temperature and stress (Krooss et al. 2002; Chalmers and Bustin 2007; Ross and Bustin 2009; Ji et al. 2012; Zhang et al. 2012; Gasparik et al. 2014; Rexer et al. 2014; Merkel et al. 2015; Yang et al. 2015, 2017; Gaus et al. 2021). In recent studies, positive correlations among sorption capacity, total organic carbon content (TOC) and micropore volume were found in organic-rich shales (Chalmers and Bustin 2007; Ross and Bustin 2009; Rexer et al. 2014; Yang et al. 2017). Ross and Bustin (2009) and Zhang et al. (2012) demonstrated that sorption capacities normalized to TOC increase with thermal maturity for

Devonian–Mississippian shales from northern British Columbia and Mississippian Barnett shale from the Fort Worth Basin. This was attributed to an increased micropore volume in the organic matter or an increase of aromaticity of the kerogen residue. Gasparik et al. (2014) and Yang et al. (2015) further observed a reverse trend at a vitrinite reflectance higher than 2.4% (dry gas stage) on Carboniferous shales from northern Germany and the Netherlands and on the Silurian Longmaxi shale from the Sichuan Basin. This could potentially result from an increasing carbonization of the organic matter and an associated destruction of micropores therein (Yang et al. 2015). With regard to the organic matter type, a decreasing trend of sorption capacity following the order: type III > type II > type I organic matter was observed (Clarkson and Bustin 1996; Zhang et al. 2012), which could be interpreted as either an increasing trend of kerogen aromaticity (Zhang et al. 2012) or a higher amount of microporous vitrinite potentially providing more sorption sites (Chalmers and Bustin 2007). Clay minerals generally feature relatively high specific surface area and the corresponding sorption capacities increase in the following order: illite < chlorite < kaolinite < I–S mixed layer < smectite (Ji et al. 2012). Moisture negatively influences sorption capacity by predominantly occupying polar sorption sites, which could otherwise be occupied by methane molecules (Gasparik et al. 2014; Merkel et al. 2015; Yang et al. 2017).

The main objective of this study is to investigate gas storage capacities (porosity and sorption capacity) and controlling mechanisms of over-mature Ediacaran (Doushantuo and Liuchapo formations) shales and to compare them with the widely characterized Lower Silurian (Longmaxi formation) shales from the Upper Yangtze platform.

2 Geological setting

The shale samples studied originate from the Upper Yangtze platform (UYP), South China (Fig. 1). The basement of the Yangtze platform is mainly composed of Neoproterozoic epimetamorphic rocks that were formed at 0.75–0.82 Ga (Charvet 2013; Ren et al. 2013). A stable platform formed and consolidated after the Jinning orogenic movement (Wang and Tan 1994). During the Ediacaran—Cambrian transition, a large-scale uplift (Tongwan movement) led to the creation of an unconformity (Tan et al. 2013; Wu et al. 2016; Fig. 2). Inner shelf, outer shelf, slope and basin were distributed in sequence from northwest to southeast during that time interval (Fig. 1; Guo et al. 2007). During the Late Ordovician to Early Silurian, the Yangtze platform gradually evolved into a foreland basin, accumulating large volumes of sediment. During this time interval, graptolite-rich shales were formed (Wufeng and Longmaxi formations; Zhai et al. 2018). Since the end of the Middle Silurian, two major uplift and erosion events largely affected the upper Yangtze platform. The first event was caused by the late Caledonian movement and lasted for 120 Ma. Erosion thickness within the southeastern Sichuan Basin is estimated to be between 100 and 200 m (Yuan et al. 2013). The second event is ongoing since the Late Cretaceous and causes another continuous uplift and erosion of the upper Yangtze platform. Deng et al. (2009) utilized apatite fission track dating to investigate the thermal uplift history of the Sichuan Basin from the Late Cretaceous onwards and estimated erosion thicknesses in southeastern Sichuan Basin to be approximately 3000 m.

3 Samples and experiments

3.1 Samples

In this study, six Ediacaran shale samples were retrieved from cores taken from depth intervals of 1047 to 1170 m during drilling operations of well ST-101 in the Songtao district of the Northeastern Guizhou Province (Table 1, Fig. 1). Sample IDs are sorted according to the order of TOC content. Samples E2 and E5 belong to the lower Doushantuo Formation and E1, E3, E4 and E6 are part of the upper Liuchapo Formation (Fig. 2). The study area is located on the slope belt between the carbonate platform and the basin (Fig. 1). For comparison, six shale samples of the Lower Silurian Longmaxi Formation were collected from the Guizhou, Hubei and Sichuan Provinces. Samples S1 and S5 were cored from intervals of approximately 600 m during drilling operations of well XY-1 in the Northern Guizhou Province. S2–S4 and S6 were collected about 0.5 m below the surface to minimize the weathering effect.

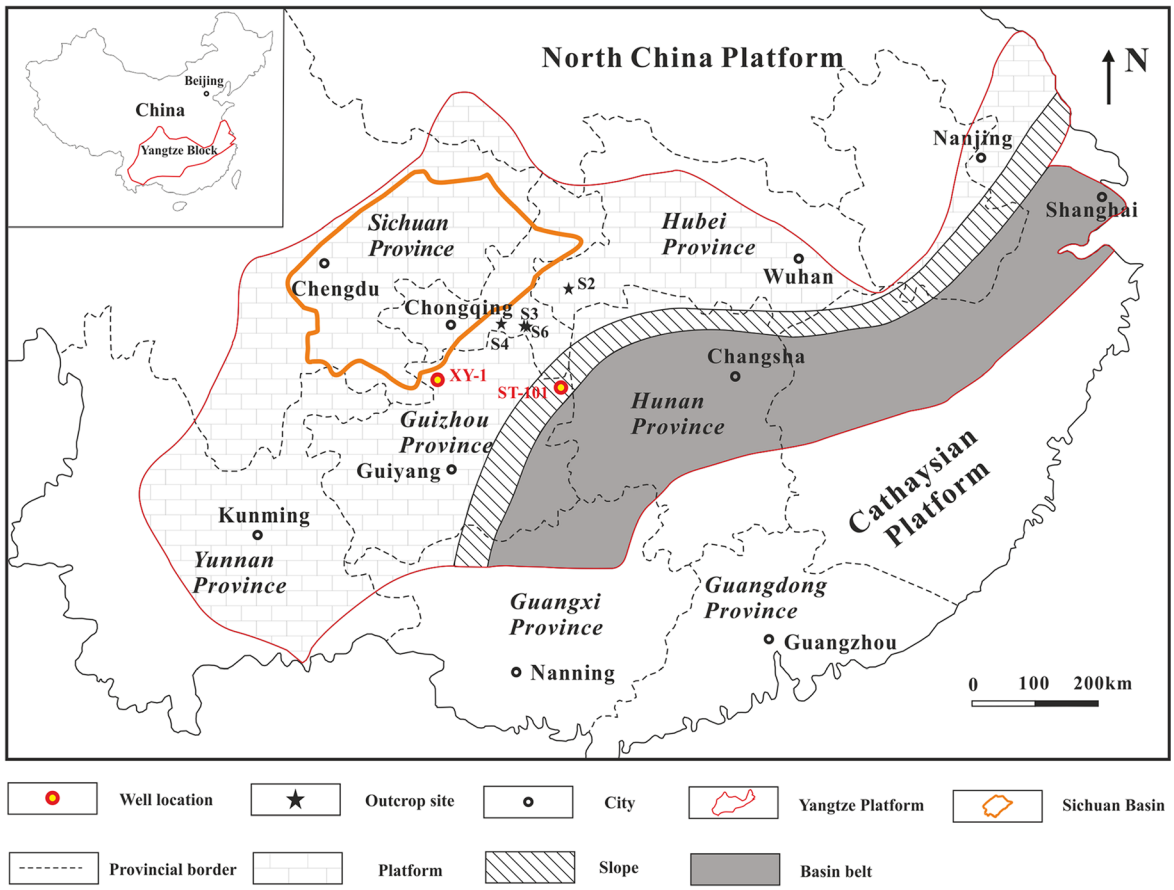

Fig. 1 Paleogeographic map of the Yangtze Platform during Ediacaran and Cambrian times (modified after Guo et al. 2007). Well ST-101 penetrated the Ediacaran Doushantuo and Liuchapo formations at depths between 1000 and 1200 m and well XY-1 intersected the Silurian Longmaxi formation at depths between 430 and 620 m

3.2 Microscopy

Sample sections were cut perpendicular to bedding and embedded in epoxy resin. The upper surfaces of the epoxy resin were ground flat and the exposed sample surfaces were subsequently polished. Solid bitumen reflectance was measured on a Zeiss Axio Imager microscope incorporated with a tungsten-halogen lamp (12 V, 100 W), a 50 × /0.85 Epiplan-NEOFLUAR oil immersion objective and a 546 nm filter. Cubic zirconium (3.125% in reflectance) was selected as the mineral standard for calibration. Since pre-Silurian shales generally do not contain vitrinite, solid bitumen was used as a substitute. Solid bitumen and vitrinite reflectance were correlated according to Eq. 1 after Mählmann and Frey (2012). Details of the measurement procedures and guidelines are found in Taylor et al. (1998) and Littke et al. (2012).

$$BR_r = -0.519 + 1.341 * VR_r - 0.0977 * (VR_r)^2 + 0.0151 * (VR_r)^3 \quad (1)$$

Here, VR_r (%) and BR_r (%) represent the equivalent vitrinite and solid bitumen reflectance.

3.3 Elemental analysis

A liquiTOC II analyser was utilized to measure total organic (TOC) and total inorganic carbon (TIC). This apparatus continuously records the CO_2 release in a phased heating process. Based on the theory that TOC and TIC are released at different temperature ranges, organic and inorganic carbon can be separately detected in a single analytical run. A Leco S200 analyser (detection limit of 0.002%) was used for the measurements of total sulphur (TS) content.

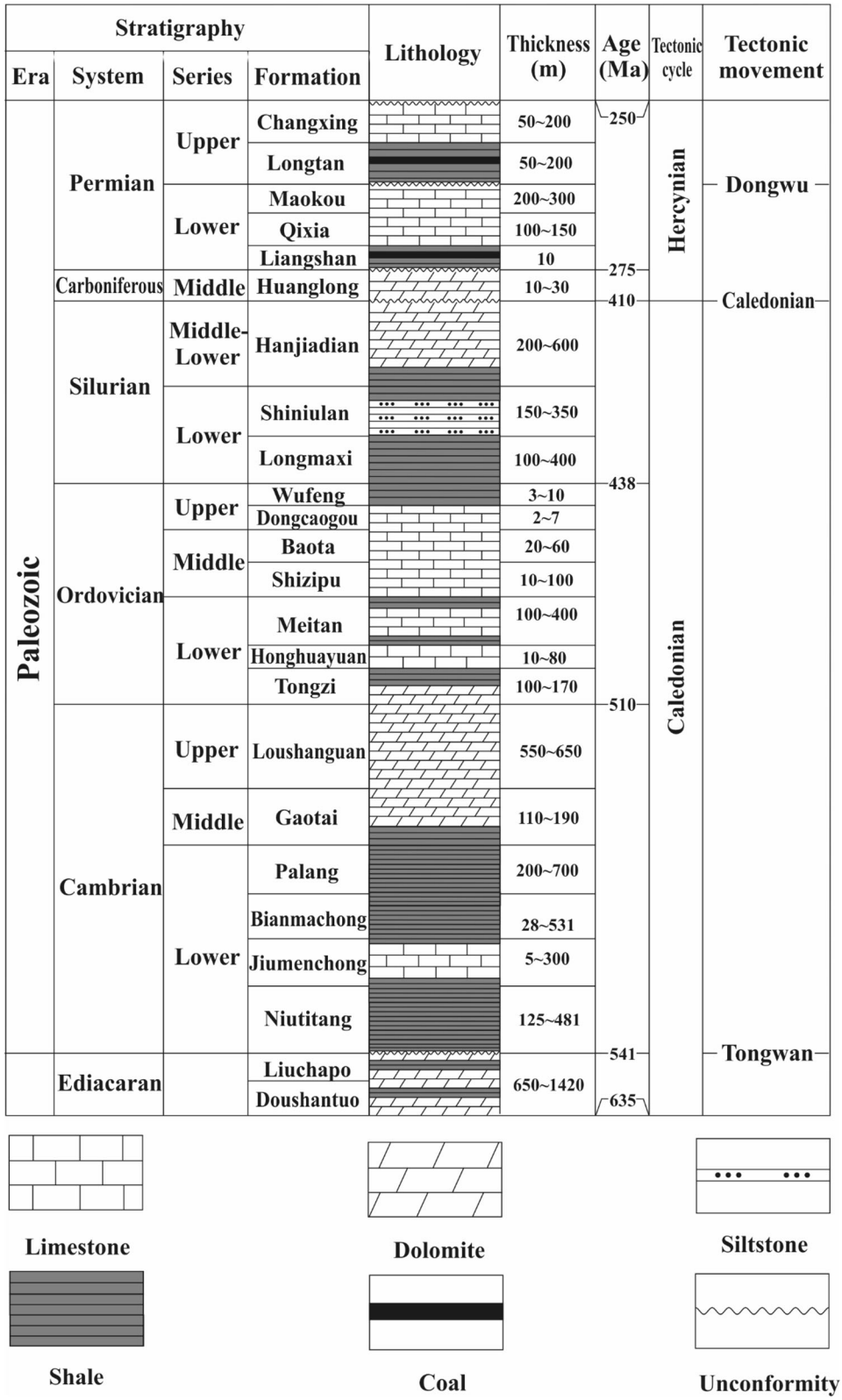
Stratigraphy
Era
System
Series
Formation
Lithology
Thickness (m)
Age (Ma)
Tectonic cycle
Tectonic movement
Paleozoic
Permian
Upper
Changxing
50~200
Longtan
50~200
Lower
Maokou
200~300
Qixia
100~150
Liangshan
10
Carboniferous
Middle
Huanglong
10~30
Silurian
Middle-Lower
Hanjiadian
200~600
Lower
Shiniulan
150~350
Longmaxi
100~400
Ordovician
Upper
Wufeng
3~10
Dongcaogou
2~7
Middle
Baota
20~60
Shizipu
10~100
Lower
Meitan
100~400
Honghuayuan
10~80
Tongzi
100~170
Cambrian
Upper
Loushanguan
550~650
Middle
Gaotai
110~190
Lower
Palang
200~700
Bianmachong
28~531
Jiumenchong
5~300
Niutitang
125~481
Ediacaran
Liuchapo
Doushantuo
650~1420
250
275
410
438
510
541
635
Hercynian
Caledonian
Caledonian
Dongwu
Caledonian
Tongwan
Limestone
Dolomite
Siltstone
Shale
Coal
Unconformity

◀**Fig. 2** Litho- and chrono-stratigraphy of the Upper Yangtze Platform (modified after Zhai.1987 and Zhang et al. 2019)

3.4 X-ray diffraction analysis (XRD)

X-ray powder diffraction (XRD) was used for quantification of the mineral composition. A particle fraction greater than 400 µm was gently crushed in a mortar and 0.2 g/g of Baikowski α-Al2O3 were added as an internal standard serving as quantification control. To avoid excess strain, heat damage and mineral dissolution, a McCrone micronizing mill was used for 15 min with ethanol as coolant. The suspension was air-dried and homogenized in a mortar before the powder bed was prepared via a top-fill procedure. XRD powder patterns were measured on a Bruker D8 using Cu Kα radiation (40 kV, 40 mA). Mineral quantification was conducted by means of Rietveld refinement using the BGMN based software Profex (Doebelin and Kleeberg 2015). For clay mineral quantification, customized clay mineral structures were used (Ufer et al. 2008; Ufer and Kleeberg 2015).

In addition to the bulk mineralogical analysis, oriented clay samples were prepared for four selected samples (E4, E5, S1 and S5). Before the clay fraction was separated through sedimentation, carbonates and organic matter were removed. Quantitative carbonate removal was achieved by hydrochloric acid treatment. The pH was adjusted to approximately 4.8 by a buffer mixture of Na-acetate and acetic acid. Organic matter was oxidized at alkaline conditions (pH of 9.5) at room temperature using sodium hypochlorite as suggested by Mikutta et al. (2005). Prior to size fractionation, excess salts were removed by extensive flushing to reduce the ionic strength of the suspension and to ensure unhindered settling of the clay fraction in the Atterberg cylinders. After enrichment of the clay-size fraction, oriented clay samples were produced from suspensions using distilled water. For qualitative identification of the particular clay mineral, oriented clay samples of (i) pure samples, (ii) samples treated with glycerol and (iii) heated samples were measured on a Bruker D8 using Cu Kα radiation (40 kV, 40 mA), respectively.

3.5 Water immersion porosimetry (WIP)

Water immersion porosimetry (WIP) based on Archimedes' principle was utilized to obtain information on the pore volume of irregular-shaped specimens. The difference in weight of the dry specimen (W_{dry}) and the fully water-saturated specimen in air (W_{sat}), together with the water density, allow for determination of the pore volume (V_{pore}; Eq. 2). The bulk volume (V_{bulk}) is derived from the difference in weight of the water-saturated specimen in air (W_{sat}) and the water-saturated specimen immersed in water (W_i; Eq. 3). The porosity equals the ratio of pore to bulk volume. A detailed discussion on the operation of WIP is given in Kuila et al. (2014) and Hu et al. (2020b).

$$V_{pore} = \frac{W_{sat} - W_{dry}}{\rho_w} \tag{2}$$

$$V_{bulk} = \frac{W_{sat} - W_i}{\rho_w} \tag{3}$$

3.6 High-pressure methane sorption measurements

To remove moisture, crushed samples (63–354 µm) were initially dried in a vacuum oven at 378.15 K until weight equilibration for at least 24 h. Subsequently, high-pressure methane sorption measurements were carried out in a manometric setup at 318.15 K and pressures up to 20 MPa. In this apparatus, the reference cell volume consists of the dead volume of the capillary volume among valve 4 (V4), valve 5 (V5) and the pressure transducer (Fig. 3). The volumes of both sample and reference cells were pre-calibrated and a leak test was performed before each sorption measurement. Leak tests were conducted with helium at 20 MPa and a leak rate < 500 Pa/h was achieved prior to measuring. Hereafter, the void volume of the filled sample cell was calibrated by helium expansion. Similar to the procedure of void volume calibration, the methane sorption measurement was programmed by sequentially transferring methane molecules from the reference cell into the sample cell until the final equilibrated pressure was reached. In the measurement, a syringe pump (Teledyne ISCO 260D) was programmed to stepwise increase the gas pressure in the reference cell.

Table 1 Characterization of Ediacaran and Silurian shale samples based on elemental composition (TOC, TS), solid bitumen reflectance (BR_r), equivalent vitrinite reflectance (VR_r) and mineral composition

Sample ID*[1]	Well/ Outcrop location	Formation	Depth (m)	Lithofacies	TOC (wt.%)	TS (wt.%)	BR_r / VR_r*[2] (%)	Mineral composition (wt.%)					
								Quartz	Feldspar	Clay + Mica	Pyrite	Carbonate	Anatase + Rutile
E1	Well ST-101	Liuchapo	1047.3	Grey massive mudstone with pyrite	1.0	1.4	3.8/ 3.6	77.6	7.0	14.0	1.4	0.0	–
E3	Well ST-101	Liuchapo	1057.2	Black massive mudstone	3.6	1.3	3.7*/ 3.5	65.2	8.9	21.3	4.4	0.2	–
E6	Well ST-101	Liuchapo	1082.2	Black massive mudstone	7.9	2.5	3.8*/ 3.6	57.6	13.3	20.4	3.7	5.0	–
E4	Well ST-101	Liuchapo	1104.2	Black massive mudstone	3.7	3.4	3.6*/ 3.5	32.8	14.9	42.1	3.7	6.6	–
E5	Well ST-101	Doushantuo	1160.8	Black massive mudstone	6.1	5.6	3.8*/ 3.7	23.5	21.9	39.6	9.1	5.9	–
E2	Well ST-101	Doushantuo	1170.0	Black massive mudstone	2.9	2.7	3.9*/ 3.7	62.3	8.0	25.8	3.0	0.9	–
S5	Well XY-1	Longmaxi	597.0	Black massive mudstone	5.2	1.1	2.9*/ 2.9	52.1	8.1	34.1	2.0	3.7	0.0
S1	Well XY-1	Longmaxi	612.0	Black laminated shale with graptolite	1.2	0.9	3.0/ 3.0	24.2	9.0	55.9	1.7	8.3	0.9
S2	Hubei	Longmaxi	0	Black massive mudstone	2.5	0.1	2.1*/ 2.1	55.1	15.5	28.3	0.0	0.0	1.7
S4	Chongqing	Longmaxi	0	Black massive mudstone	4.0	0.2	2.0/ 2.1	70.6	5.1	23.4	0.0	0.0	0.9
S3	Chongqing	Longmaxi	0	Black massive mudstone with calcite strip	3.2	1.0	2.8/ 2.8	28.7	10.6	24.3	1.0	35.5	0.0
S6	Chongqing	Longmaxi	0	Black massive mudstone	6.6	0.5	2.8/ 2.8	62.3	10.6	26.2	0.0	0.0	0.9

*[1]Sample IDs are sorted according to the order of TOC content

*[2]Solid bitumen reflectances were taken from Zhang et al. (2019) and converted to vitrinite reflectances by using Eq. 1 after Mählmann and Frey (2012)

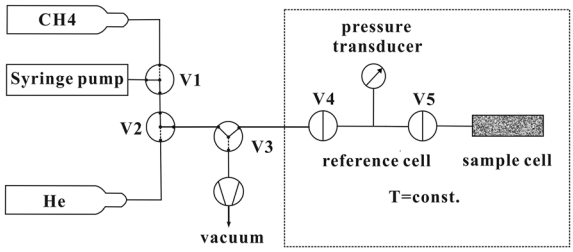

Fig. 3 High-pressure sorption setup (V1-V5 are either two-port or three-port valves and the syringe pump (Teledyne ISCO 260D) was programmed to stepwise increase the gas pressure in the reference cell)

The excess sorption amount (n_{excess}) corresponds to the difference between the entire amount of gas transferred from the reference cell into the sample cell (n_{trans}) and the amount of "free" gas occupying the void volume (V_{void}) of the sample cell.

$$n_{excess}(P,T) = n_{trans}(P,T) - \rho_g(P,T) \cdot V_{void} \tag{4}$$

The pressure- and temperature-dependent methane density (ρ_g; kg/m^3) was computed using the GERG equation of state (EOS; Kunz and Wagner 2012).

Considering potential systematic errors of temperature and pressure recordings, for example, due to the impurity of methane or the interaction between methane molecules and the internal surface of the apparatus, a blank measurement with methane is particularly important to generate reproducible isotherms when different setups are used (Gasparik et al. 2014). Therefore, stainless steel balls of known volume were used instead of the actual shale samples. The derived "blank" isotherm was subtracted from measured excess sorption isotherms of the actual samples. The "blank-corrected" isotherms could be described by a Langmuir-type function (Eq. 5),

$$n_{excess}(P,T) = n_{\infty}\frac{P}{P+P_L(T)}\left(1-\frac{\rho_g(P,T)}{\rho_a}\right) \tag{5}$$

Here, $n_{excess}(P,T)$ (mmol/g) represents the "blank-corrected" excess amount of methane at pressure P (Pa) and temperature T (K). n_{∞} (mmol/g) and P_L (Pa) represent the Langmuir volume and Langmuir pressure, respectively. ρ_a (kg/m^3) and ρ_g (P,T) (kg/m^3) are the densities of the sorbed and free gas at P and T. In this study, the sorbed phase density is kept constant at 423 kg/m^3 (liquid methane density at 10^5 Pa and 111.65 K) to reduce the amount of adjustable parameters (Dreisbach et al. 1999).

Additionally, two dry Ediacaran samples (E4 and E6) were moisturized in a desiccator with a super-saturated K_2SO_4 solution to ensure 97% relative humidity (RH) at 293.15 K. After the sample weights remained constant, sorption measurements were repeated on these moisture-equilibrated samples.

Based on the experimental data, the in-situ excess sorption capacity at specific temperatures can be estimated (Eq. 5). The free gas capacity can also be calculated with porosity, bulk rock density and in-situ free gas density (Eq. 6). Thus, the GIP amount equivalent to the sum of free gas and excess sorption capacities can be estimated by setting of the following parameters (Eq. 7).

$$G_f = \frac{\phi\rho_g(P,T)}{M\rho_{bulk}} \tag{6}$$

$$\begin{aligned} GIP &= G_{ex} + G_f \\ &= n_{\infty}\frac{P}{P+P_L(T)}\left(1-\frac{\rho_g(P,T)}{\rho_a}\right) + \frac{\phi\rho_g(P,T)}{M\rho_{bulk}} \end{aligned} \tag{7}$$

Here, GIP (mmol/g), G_{ex} (mmol/g) and G_f (mmol/g) represent the total amount of gas storage, excess sorption capacity and free gas capacity, respectively. ϕ (-), ρ_{bulk} (kg/m^3) and M (g/mol) denote the porosity and bulk density of the shale as well as molar mass of methane, respectively.

3.7 Low-pressure nitrogen and carbon dioxide adsorption measurements

These measurements were performed on a dry 200–400 μm particle-size fraction of the bulk sample material using the manometric Gemini VII 2390t setup (Micromeritics Instrument Corporation, Norcross, GA, USA). Firstly, samples were evacuated at 378 K for at least 16 h in a VacPrep 061 to remove liquids occupying the pore space (Micromeritics Instrument Corporation, Norcross, GA, USA). To obtain N_2 isotherms, the amounts of N_2 adsorbed at 93 discrete pressure points between 0.001 and 0.995 p/p^0 were measured at 77 K in a cryogenic nitrogen bath. The saturation pressure (p^0) was determined separately for each pressure point and operational equilibrium was assumed at a pressure drop of less than 0.01% over a time interval of 30 s. To assess the micropore volume, CO_2 sorption isotherm measurements were performed

at 273 K at 25 discrete pressure steps between 0.001 and 0.036 p/p^0. The highest measurable partial pressure was restricted to 0.036 due to the high saturation pressure (3.49 MPa) of carbon dioxide at operational temperature. An equilibrium criterion of 10 s was applied assigning equilibrium when the pressure fluctuates less than 0.01% over the given time.

The pore structure was characterized by traditional physisorption theories including Brunauer–Emmett–Teller (BET) theory for specific surface area quantification, Barrett–Joyner–Halenda (BJH) theory for pore volume distribution calculation, Gurvich's rule (GV) for total pore volume assessment and Dubinin-Astakhov theory (DA) for micropore volume determination (Gurvich 1915; Brunauer et al. 1938; Barrett et al. 1951; Dubinin and Astakhov 1971). Detailed explanation of the fundamentals of the individual theories can be found in Rouquerol et al. (2013) and references therein.

4 Results

4.1 Mineral composition

XRD analysis results of Ediacaran and Silurian shales are listed in Table 1. For both shales, quartz is the dominating phase ranging from 23.5 to 77.6 wt.%, followed by clay minerals ranging from 14.0 to 55.9 wt.% and feldspars ranging from 5.1 to 21.9 wt.%. Minor contributions (< 10 wt.% on average) of carbonates and pyrite as well as traces of anatase and rutile (heavy minerals) were detected as well. The average brittle mineral content (quartz + feldspar + carbonates) of Ediacaran shales (68.6 wt.%) is higher than that of Silurian shales (66.5 wt.%), while the average clay content of Ediacaran shales (27.2 wt.%) is lower than that of Silurian shales (32.0 wt.%). Based on the texture preparations, clay types were qualitatively distinguished (appendix 1). Whereas illite/muscovite was the only identified clay type in the Ediacaran shales, illite/muscovite and chlorite were distinguished for the Silurian shales.

4.2 TOC, TS and thermal maturity

TOC contents of the Ediacaran and Silurian shales vary from 1.0 to 7.9 wt.% (4.2 wt.% on average) and 1.2 to 6.6 wt.% (3.8 wt.% on average), respectively (Table 1). TS contents of the Ediacaran shales (1.3–5.6 wt.%) are generally higher than those of the Silurian shales (0.1–1.1 wt.%). The equivalent vitrinite reflectances of Ediacaran shales range between 3.5 and 3.7% (dry gas stage; Table 1). Values of Longmaxi shales are lower and range between 2.1 and 3.0% (dry gas stage).

Due to the difference of dissolved sulfate concentration between marine and fresh water environments, the TOC/TS ratio is a useful parameter to distinguish organic-rich fresh water from marine sediments (Berner and Raiswell 1984). Considering the loss of organic matter during maturation, the TS content was plotted against 2 × TOC content (Uffmann et al. 2012; Fig. 4). A majority of the shale samples distribute along the "normal marine" line, while three Silurian shales (S2, S4 and S6) display a significantly lower TS/TOC ratio. These samples were taken from outcrops and therefore possibly subjected to weathering, which likely led to relative enrichment of TOC when compared to TS (Littke et al. 1991).

4.3 Pressure equilibration and uptake kinetics

Pressure equilibration is a prerequisite to study storage properties in shales by gas expansion methods such as helium pycnometry and high-pressure methane sorption. Therefore, it was closely monitored during this study (Fig. 5). Equilibration times for all samples with similar particle sizes (between 64 and 354 µm) are exemplarily shown for equilibrated methane pressures of ~ 0.5 MPa (Fig. 5a and b) and range between 49 to 292 min and 20 to 150 min for the Ediacaran and Silurian shales, respectively. Helium uptakes were generally faster than methane uptakes as is exemplarily shown for sample E1 at approximately equivalent mean gas pressures of 0.5 MPa (Fig. 5c) and equilibration times decrease with increasing mean gas pressure which is exemplarily shown for sample E2 with methane pressures from 0.7 to 20.5 MPa (Fig. 5d).

4.4 High-pressure methane sorption

Methane sorption isotherms at dry and moist conditions were measured at 318.15 K (approximately equivalent to current in-situ temperatures of the Ediacaran samples) (Fig. 6). For all samples measured in the dry state, experimental results demonstrate a

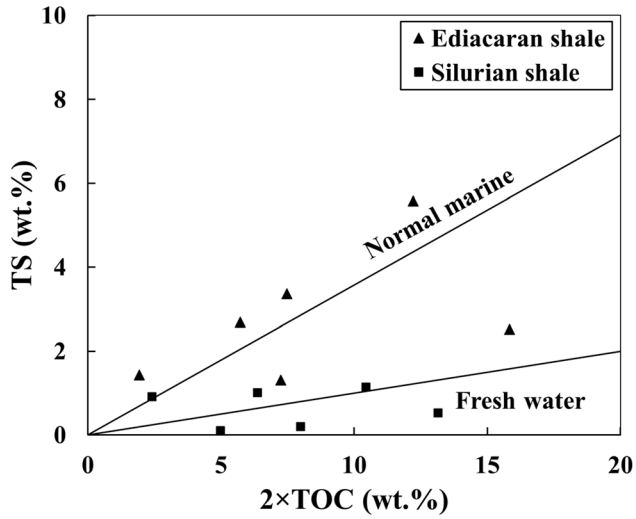

Fig. 4 Relationship between TS and TOC content (multiplied by 2) for Ediacaran and Silurian shale samples ("normal marine" and "fresh water" line after Berner and Raiswell.1984)

wide variation in the maximum excess methane sorption capacity (0.016–0.135 mmol/g). All excess sorption isotherms obtained at dry conditions are similar in shape and exhibit maxima between 9 and 14 MPa methane pressure. Therefore, Eq. 5 was used to fit the experimental results. Fitted Langmuir pressures and Langmuir volumes normalized to either sample weight or sample weight and TOC content are listed in Table 2. Langmuir pressures of the Silurian shales, ranging from 3.12 to 8.42 MPa (5.63 MPa on average), are higher than the Ediacaran shales with values ranging from 2.05 to 5.19 MPa (3.56 MPa on average). Langmuir volumes normalized to sample weight range between 0.02 and 0.19 mmol/g (0.10 mmol/g on average) and 0.08–0.21 mmol/g (0.13 mmol/g on average) for the Ediacaran and Silurian shales, respectively. A positive correlation between Langmuir volumes and TOC contents was identified for both shales (Fig. 7). The Ediacaran samples E4 and E6 were additionally moisturized at a relative humidity of 97%. Equivalent water contents were 2.1 and 3.1 wt.% and Langmuir volumes decreased by 32 and 48%, respectively (Table 2). The decrease in excess sorption capacity at 10 MPa methane pressure ranges from 61 to 64%.

4.5 Low-pressure nitrogen adsorption

According to the IUPAC classification, N_2 adsorption isotherms of all samples can be described by a Type IV isotherm that is characteristic of a hysteresis loop (Thommes et al. 2015; Fig. 8a and b). The preliminary phase of fast adsorption accumulation with pressure results from micropore filling followed by monolayer-multilayer adsorption of N_2. As the pressure decreases, the desorption branch falls abruptly forming a hysteresis loop with the adsorption branch. The hysteresis loops of the studied shales belong to Types H3 and H2 (Seemann et al. 2017). The closure points of hysteresis loops in Type IV isotherms generally arise at a lower relative pressure of 0.42, which depends on the adsorptive and the pore structure (Thommes et al. 2015; Yang et al. 2015; Seemann et al. 2017). However, closure points of most of the samples occur at relative pressures lower than 0.42. This low-pressure hysteresis (LPH) indicates incomplete equilibrium and can be attributed to slow diffusion in ultra-micropore space. BET specific surface areas of the Ediacaran and Silurian samples range from 1.19 to 24.32 m^2/g (10.20 m^2/g on average) and 5.45 to 24.86 m^2/g (17.27 m^2/g on average), respectively. No correlation was observed between BET specific surface area and TOC content (Fig. 9a).

4.6 Porosity and pore size distribution

WIP porosity values of the Ediacaran shales range from 1.4 to 4.6% (3.5% on average; Table 3). WIP porosities of the Silurian shales (excluding weathered samples S2, S4 and S6) are higher, ranging from 6.2 to 7.4% (6.8% on average). Correspondingly, the average specific pore volumes of Ediacaran and Silurian shales are 0.0135 and 0.0271 cm^3/g, respectively.

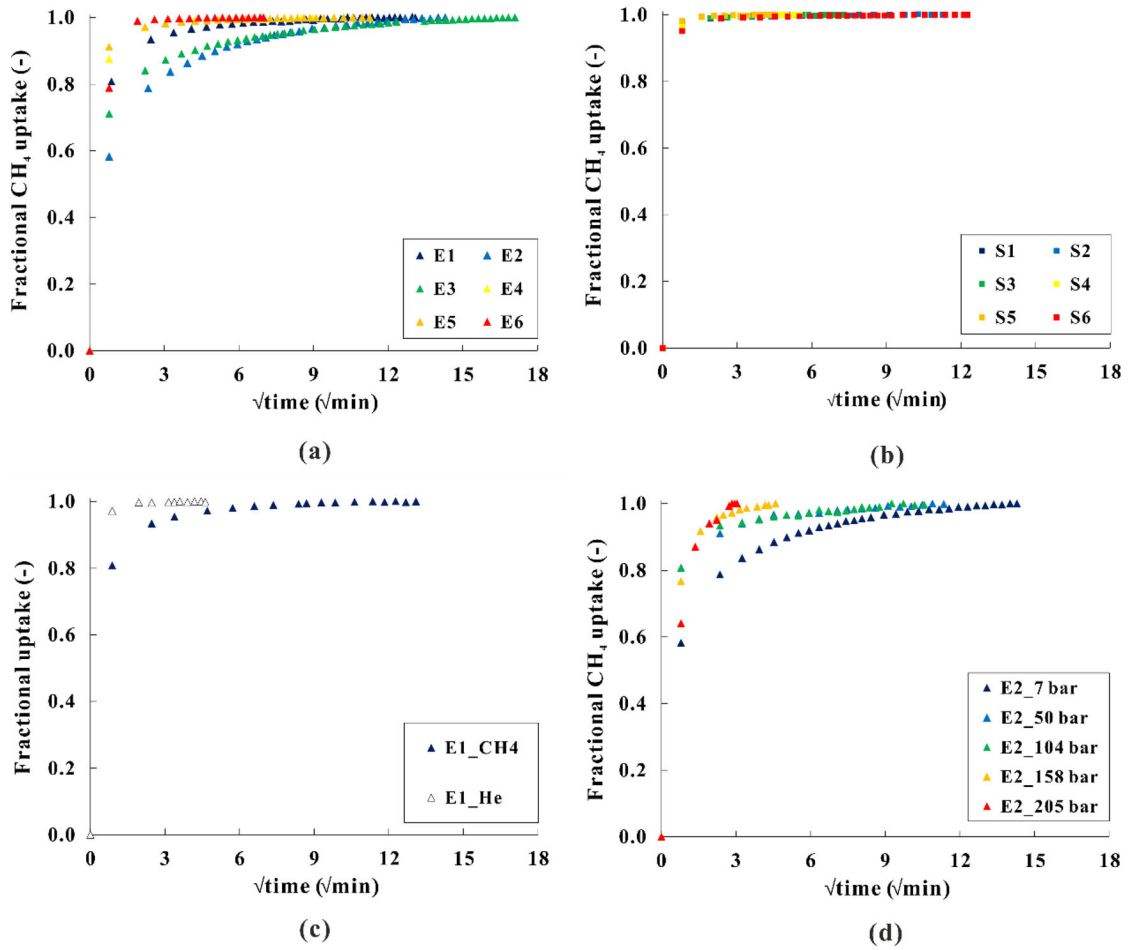

Fig. 5 Fractional uptake versus square root of time for **a** Ediacaran and **b** Silurian shales at about 0.5 MPa methane pressure, **c** helium and methane uptake rates of sample E1 at about 0.5 MPa gas pressure and **d** uptake rates at varying methane pressures from 0.7 to 20.5 MPa for sample E2

Interpretation of N_2 adsorption isotherms using the BJH theory shows that the pore sizes range between 1.6 and 153 nm for all samples (Fig. 10a and b). The mesopore volume of the Silurian shales, varying between 0.0058 and 0.0200 cm^3/g (0.0135 cm^3/g on average), is approximately two times larger than that of the Ediacaran shales with values varying between 0.0025 and 0.0118 cm^3/g (0.0070 cm^3/g on average; Table 3). Based on the interpretation of CO_2 adsorption branch data using the DA theory, the derived micropore volumes of the Ediacaran shales (0.0009–0.0092 cm^3/g, 0.0054 cm^3/g in average) are in the same range as those of the Silurian shales (0.0045–0.0100 cm^3/g, 0.0066 cm^3/g on average). A positive correlation between CO_2 micropore volume and TOC content was observed for both shales (Fig. 9b). Normalized to the specific total pore volume determined by WIP, micro- and mesopores of the Ediacaran shales account for 37.9% (16.9–67.0%) and 53.5% (20.2–88.1%) on average, respectively. Excluding the weathered samples (S2, S4 and S6), the average proportions of micro- and mesopores for Silurian samples are 22.1% (17.1–26.9%) and 46.2% (34.0–60.8%), respectively.

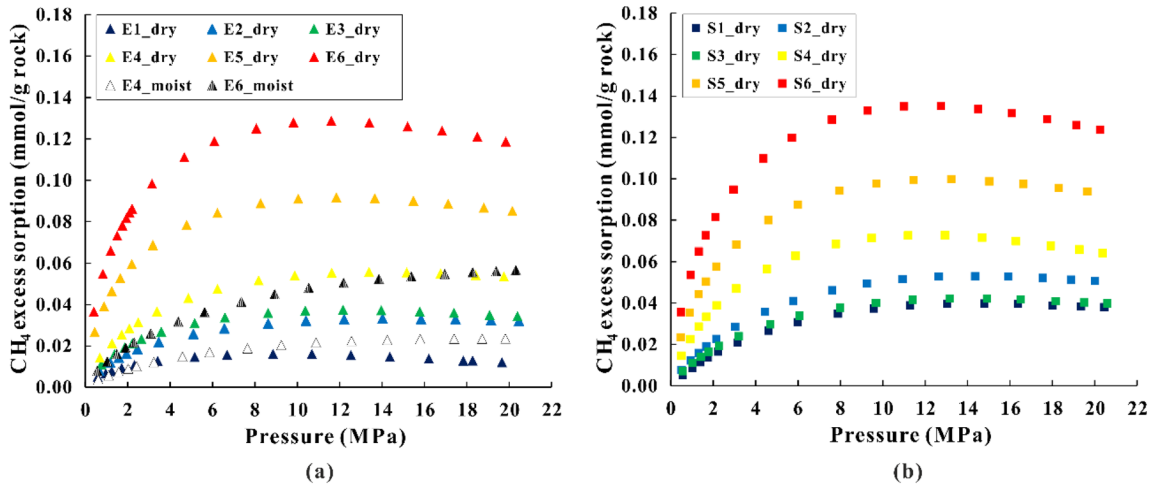

Fig. 6 Methane sorption isotherms at 318.15 K for **a** Ediacaran shales at dry and moist conditions (97% relative humidity) and **b** Silurian shales at dry conditions

Table 2 Excess sorption capacities at 10 MPa (n_{ex}^{10MPa}), Langmuir volumes (n_∞) normalized to sample weight or sample weight and TOC content as well as Langmuir pressure (P_L) for Ediacaran (E1-E6) and Silurian (S1-S6) shales at dry and moist (97% relative humidity) conditions

Sample ID	Water content (wt.%)	TOC (wt.%)	Methane excess sorption (45 °C)			
			n_{ex}^{10MPa} (mmol/g)	n_∞ (mmol/g)	n_∞(mmol/g TOC)	P_L (MPa)
E1	0	1.0	0.016	0.022	2.253	2.05
E2	0	2.9	0.032	0.059	2.065	5.19
E3	0	3.6	0.038	0.062	1.708	4.02
E4	0	3.7	0.055	0.098	2.702	4.97
E4	*2.14*	*3.7*	*0.021*	*0.051*	*1.439*	*9.84*
E5	0	6.1	0.093	0.139	2.279	2.65
E6	0	7.9	0.132	0.192	2.423	2.44
E6	*3.08*	*7.9*	*0.048*	*0.131*	*1.709*	*12.37*
S1	0	1.2	0.038	0.082	6.850	8.42
S2	0	2.5	0.051	0.105	4.221	7.49
S3	0	3.2	0.041	0.081	2.548	6.93
S4	0	4.0	0.073	0.120	3.000	4.18
S5	0	5.2	0.100	0.161	3.093	3.65
S6	0	6.6	0.137	0.211	3.210	3.12

5 Discussion

5.1 Influence of organic matter and clay minerals on methane sorption capacity

Data collected in this study suggest that sorption capacity is equally important as a storage mechanism for the Ediacaran and Silurian samples (Δ average Langmuir volume = 0.03 mmol/g, Table 2). A strong positive correlation between Langmuir volumes and TOC contents for both sample sets indicates a first-order influence of TOC content on sorption capacity. The use of low-pressure CO_2 adsorption measurements in this study additionally confirmed that

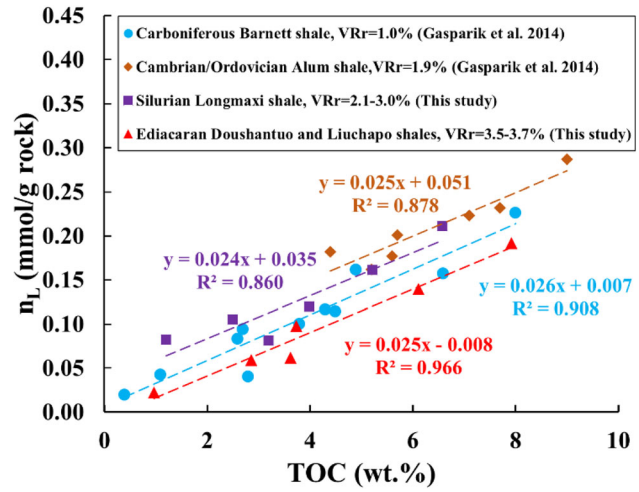

Fig. 7 Comparison of Langmuir volumes and TOC contents for samples from the Ediacaran (Doushantuo and Liuchapo shales), Silurian (Longmaxi shale), Carboniferous (Barnett shale) and Cambrian/Ordovician (Alum shale)

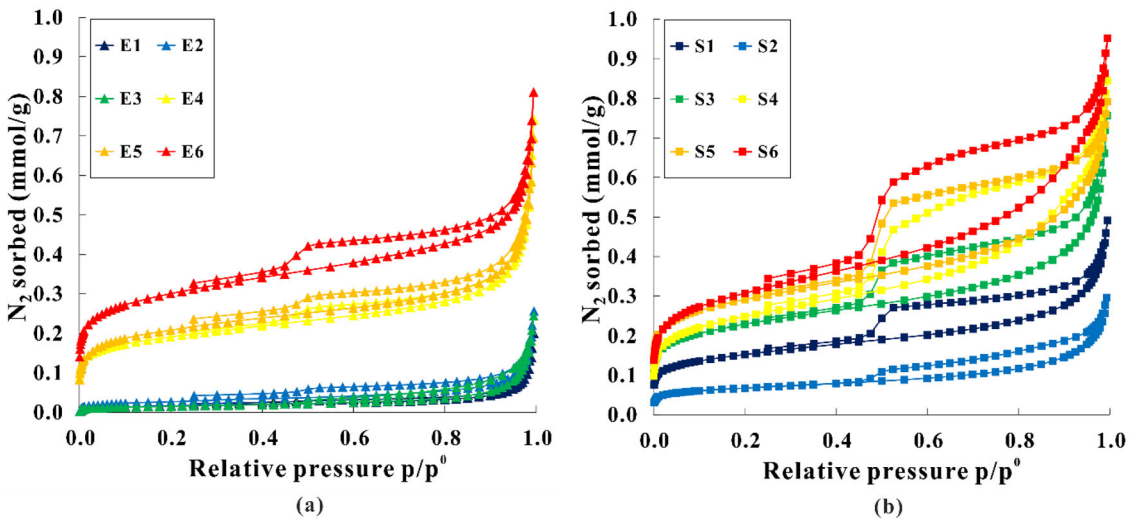

Fig. 8 Nitrogen adsorption and desorption isotherms of the Ediacaran (**a**) and Silurian (**b**) shales at 77 K

sorption predominantly occurs within organic matter micropores for both shales (positive correlation between CO_2 micropore volume and TOC in Fig. 9b). Similar results were also reported by Gasparik et al. (2014). From both figures (Fig. 7 and 9b) it is also evident that Langmuir and micropore volumes are exclusively related to the TOC content in the Ediacaran shale (linear regression to 0 wt.% TOC). For the Silurian shale, on the other hand, the linear regression yields 0.035 mmol/g rock (Fig. 7) and 0.0032 cm^3/g (Fig. 9b) at 0 wt.% TOC, indicating that not only TOC content but also inorganic minerals contain micropore volume for sorptive storage. This was additionally tested by a linear combination approach in the following form:

$$n_\infty = n_{TOC}w_{TOC} + n_{clay}w_{clay} + n_{rigid}w_{rigid} \quad (8)$$

Here, n_∞ (mmol/g) is the Langmuir volume obtained from experimental data, n_{TOC}, n_{clay}, n_{rigid} (mmol/g) represent the fitted individual Langmuir volumes of organic matter, clay minerals and rigid minerals, respectively. Correspondingly, w_{TOC}, w_{clay} and w_{rigid} denote the experimentally determined mass fractions of the rock constitutes. It should be noted that this approach was applied simultaneously to the entire

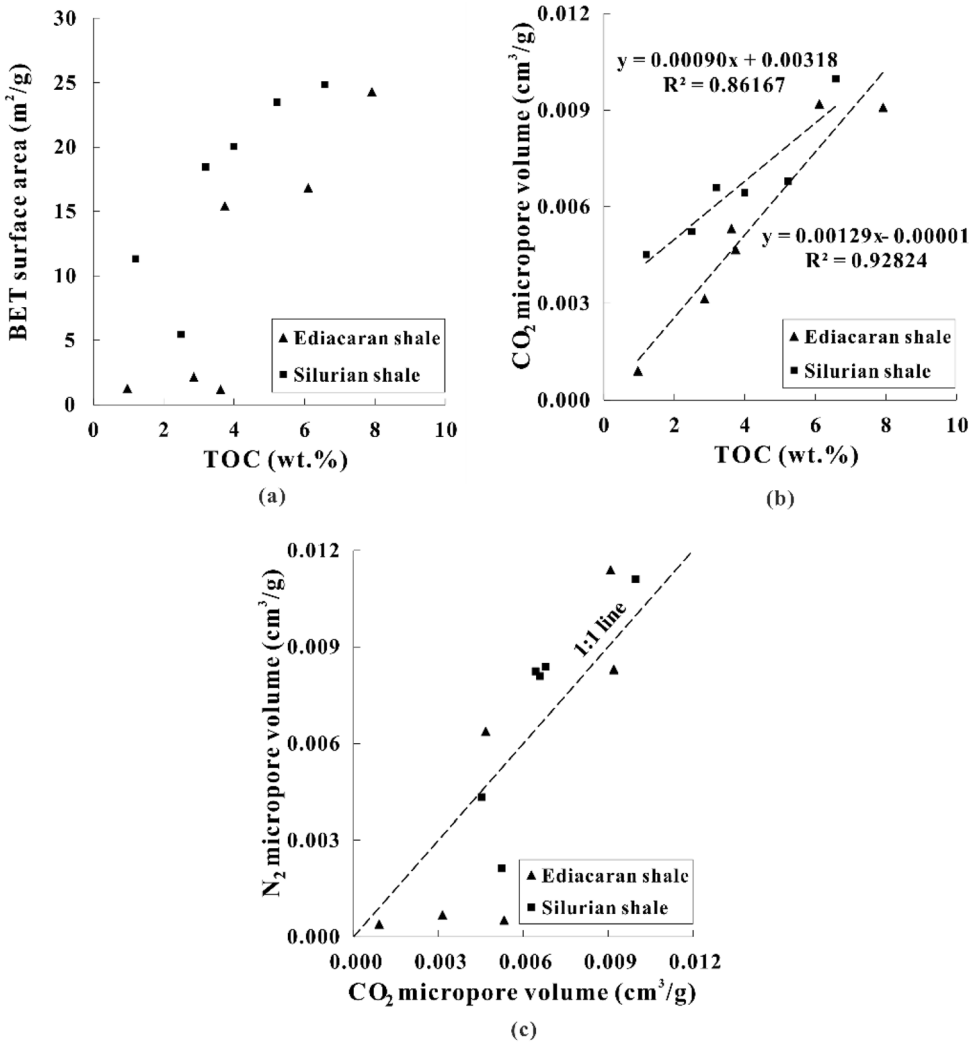

Fig. 9 Relationships between TOC content and BET surface area (**a**), TOC content and CO_2 micropore volume (**b**) and CO_2 micropore volume and N_2 micropore volume (**c**)

sample set and therefore provides a single value for n_{TOC}, n_{clay} and n_{rigid} that characterizes the entire sample set.

Results for the Ediacaran samples indicate a contribution of 2.452 mmol/g for organic matter and 0 mmol/g for clay minerals as well as rigid minerals (Fig. 11a and b). For the Silurian shales, on the other hand, estimated Langmuir volumes were 0, 0.082 and 2.834 mmol/g for rigid minerals, clay minerals and organic matter, respectively (Fig. 11c and d). Accordingly, the average contribution of clay minerals to the total Langmuir volume is $\approx$ 23% for the Silurian shales and 0% for the Ediacaran shales, although both shales have similar clay contents. Ji et al. (2012) suggested that sorption capacities for different clay mineral types vary strongly from 0.079 to 0.380 mmol/g and increase in the order of illite < chlorite < kaolinite < I–S mixed layer < smectite. Thus, higher sorption capacities of the clay fraction for the Silurian samples as compared to the Ediacaran samples could be the result of the abundance of chlorite (appendix 1). However, this does not explain as to why zero sorption was computed for the muscovite/illite phase of the Ediacaran samples. Reported maximum excess methane sorption capacities for illite range from 0.055 mmol/g to 0.13 mmol/g (Ross and Bustin 2009; Ji et al. 2012; Liang et al. 2016). McDowell and Elders (1980)

Table 3 Porosity and pore structure analysis results from N_2 and CO_2 adsorption measurements on Ediacaran (E1-E6) and Silurian (S1-S6) shale samples

Sample ID	Porosity (%)	N_2 BET specific surface area (m^2/g)	CO_2 micropore surface area (m^2/g)	CO_2 micropore volume (cm^3/g)	N_2 mesopore volume (cm^3/g)	Mesopore/micropore volume ratio	Total pore volume (cm^3/g)
E1	1.4	1.28	2.53	0.0009	0.0025	2.77	0.0053
E2	3.8	2.16	8.75	0.0031	0.0037	1.17	0.0147
E3	4.6	1.19	12.64	0.0053	0.0037	0.70	0.0183
E4	3.0	15.43	12.36	0.0047	0.0100	2.15	0.0114
E5	3.7	16.83	22.41	0.0092	0.0101	1.09	0.0137
E6	4.4	24.32	23.17	0.0091	0.0118	1.30	0.0175
Mean	3.5	10.20	13.64	0.0054	0.0070	1.53	0.0135
S1	6.7	11.33	10.90	0.0045	0.0090	1.99	0.0265
S2	14.8	5.45	14.10	0.0052	0.0058	1.11	0.0658
S3	7.4	18.45	15.98	0.0066	0.0129	1.96	0.0295
S4	10.0	20.06	17.07	0.0064	0.0180	2.80	0.0430
S5	6.2	23.50	17.25	0.0068	0.0154	2.26	0.0253
S6	9.6	24.86	23.90	0.0100	0.0200	2.01	0.0418
Mean	6.8*	17.27	16.53	0.0066	0.0135	2.02	0.0271*

*The value of average porosity or average total pore volume is calculated from samples S1, S3 and S5 considering the weathering effect to the other outcrop samples

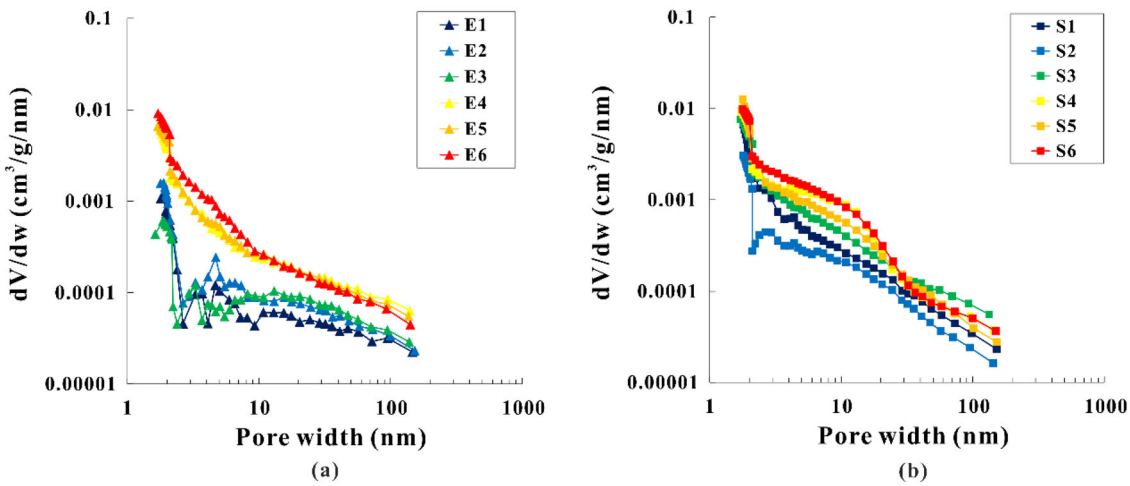

Fig. 10 Differential pore volume distribution (dV/dw) of Ediacaran (**a**) and Silurian (**b**) shales

observed that, at temperatures of approximately 548.15 K, illite/mica changes gradually from fine-grained illite to coarse-grained recrystallized mica. Such change could be accompanied by a shift of the pore size towards larger pores and therefore decreasing surface area and sorption capacity. Since the thermal history of Ediacaran samples used in this study is relatively poorly known, the use of empirical formulas to relate vitrinite reflectance to palaeotemperature has been applied as a first approximation. Depending on whether relatively slow or fast heating occurred during burial, different empirical formulations are typically used (Waliczek et al. 2021):

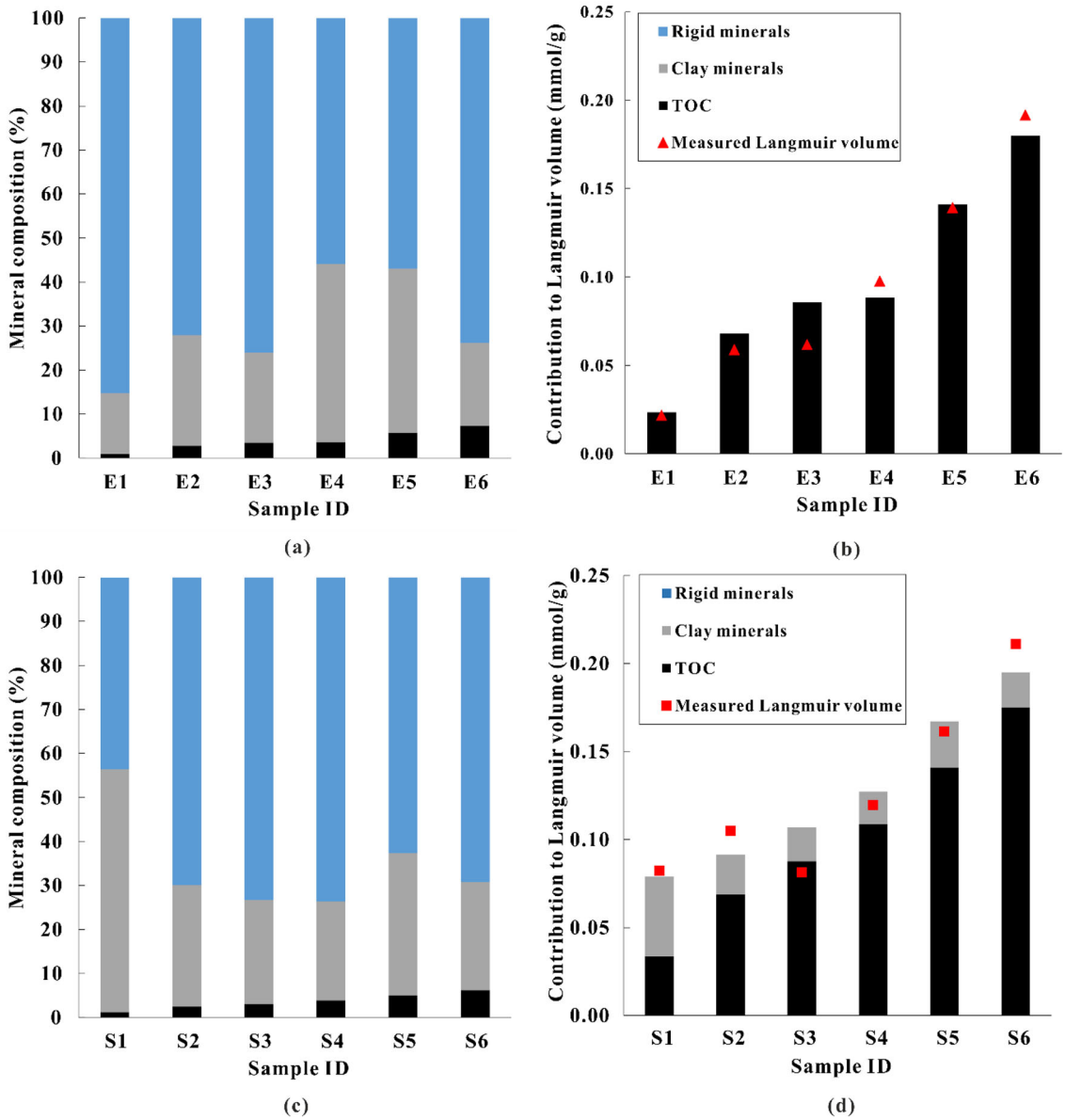

Fig. 11 Mineral composition and respective contribution to Langmuir volume for the Ediacaran (**a**, **b**) and Silurian (**c**, **d**) shales (blue, grey and black colors represent rigid minerals, clay minerals and organic matter, respectively)

$$T_{peak} = (lnVR_r + 1.68)/0.0124 \quad (9)$$

$$T_{peak} = (lnVR_r + 1.19)/0.00782 \quad (10)$$

Here, T_{peak} denotes the maximum paleotemperature (K) and VR_r denotes the measured vitrinite reflectance (%). From these empirical formulas, the temperatures were between 510.15 and 592.15 K for Ediacaran samples while 468.15–566.15 K were computed for Silurian samples. Therefore, recrystallisation in these Ediacaran samples could be responsible for altered sorption capacities. Another possibility emerges from the observations of Weaver (1967, 1989). He found that illite in Precambrian shales was likely formed by alteration of feldspar in alkaline environments whereas illite in Paleozoic shales predominantly formed by illite/smectite conversion. While illite/smectite conversion could be related to a solid-state transformation, formation of illite from feldspars is

related to dissolution and precipitation processes. This could explain differences in sorption characteristics as well but requires further in-detail studies on the origins of illite in both sample sets.

The average Langmuir pressure (5.63 MPa) of the Silurian shales was 1.6 times higher than that (3.56 MPa) of the Ediacaran shales. Zhang et al. (2012) observed a similar trend (decreasing Langmuir pressure with increasing thermal maturity) for shales, albeit at lower vitrinite reflectances (0.58%–2.01%). They attributed this phenomenon to a higher degree of aromatization of the kerogen. In this study, the Langmuir pressure difference could also be derived from differences in the pore size distribution as the average micropore volume fraction of the Ediacaran shales is approximately two times higher than that of the Silurian shales.

5.2 Influence of thermal maturity on methane sorption capacity

Several studies suggested that methane sorption capacity in shales normalized to the TOC content increases upon thermal maturation (Gasparik et al. 2014; Hu et al. 2015). Possible reasons for such an increasing sorption capacity are: (1) an increasing fraction of organic matter accommodated porosity (increasing specific surface area) due to kerogen conversion (Ross and Bustin 2009; Klaver et al. 2015) and (2) an increasing methane affinity of organic matter due to an increasing proportion of aromatic structures relative to aliphatic structures (Vandenbroucke and Largeau 2007). Additionally, it was found that methane sorption capacity normalized to the TOC content decreases in highly over-mature shales from a vitrinite reflectance of approximately 2.0–2.4% onwards (Gasparik et al. 2014; Yang et al. 2015). This was attributed to an increasing carbonization and an associated destruction of organic matter-hosted micro-pores (Yang et al. 2015). It should be noted that these studies exclusively attributed the sorption capacities (Langmuir volumes) to organic matter, thereby neglecting a potential contribution of clay minerals to total sorption capacity. While this is a valid simplification for high TOC shales and coals, the impact of clay minerals should not be neglected for shales with lower organic matter content. To exemplify the potential influence of clay minerals on the previously reported maturity trend, Eq. 8 was utilized to compute Langmuir volumes of organic matter from other published data (Gasparik et al. 2014; Yang et al. 2015; Merkel et al. 2016; Li et al. 2017; Fink et al. 2018; Nolte et al. 2019; Gaus et al. 2020) and data from this study under three different assumptions: (1) zero clay mineral contribution to total sorption capacity, (2) 0.1 mmol/g clay mineral contribution to total sorption capacity and (3) 0.2 mmol/g clay mineral contribution to total sorption capacity (Fig. 12). The three assumptions are based on computation results from chapter 5.1 and published sorption capacities for individual clay minerals (Ross and Bustin 2009; Ji et al. 2012; Ziemiański et al. 2020). Vitrinite reflectances for all sample sets used in Fig. 12 range from 0.50% to 4.24% and TOC contents from 2.2 to 45.0 wt.%. Under assumption of the minimum clay contribution (0 mmol/g, upper error bars for maximum deviations in Fig. 12) an inverted U-shaped trend of sorption capacity with increasing vitrinite reflectance is apparent as was observed by Gasparik et al. (2014) and Yang et al. (2015) from vitrinite reflectances of 0.5% to 3.72%. However, adjusting the clay mineral sorption to values of 0.1 mmol/g (intermediate contribution, individual data points in Fig. 12) and 0.2 mmol/g (maximum contribution, lower error bars for maximum deviations in Fig. 12) indicates that clay mineral contributions cannot be neglected as the shift of individual data points along the y-axis due to varying clay mineral contributions may be in the same range as the proposed inverted U-shaped trend due to thermal maturation. This is especially valid if TOC content is relatively low and the clay mineral fraction is relatively high. Results from Gaus et al. (2020) (Kimmeridge & Bazhenov shales) and Gasparik et al. (2014) (Barnett & Alum shales) in Fig. 12 display those changes in the sorption capacity due to differences in the pretreatment (different particle sizes) and due to heterogeneity, respectively, are in the same range as the proposed inverted U-shaped trend due to thermal maturation as well. Additionally, it should be noted that the thermal history can be affected by different parameters such as burial depth, uplift and erosion, basal heat flow and magmatic activity as well as physical properties of the formation (Hantschel and Kauerauf 2009). Results from Nolte et al. (2019) for shales from the Collingham and Whitehill formations from South Africa exhibit higher sorption capacities than expected, which is likely

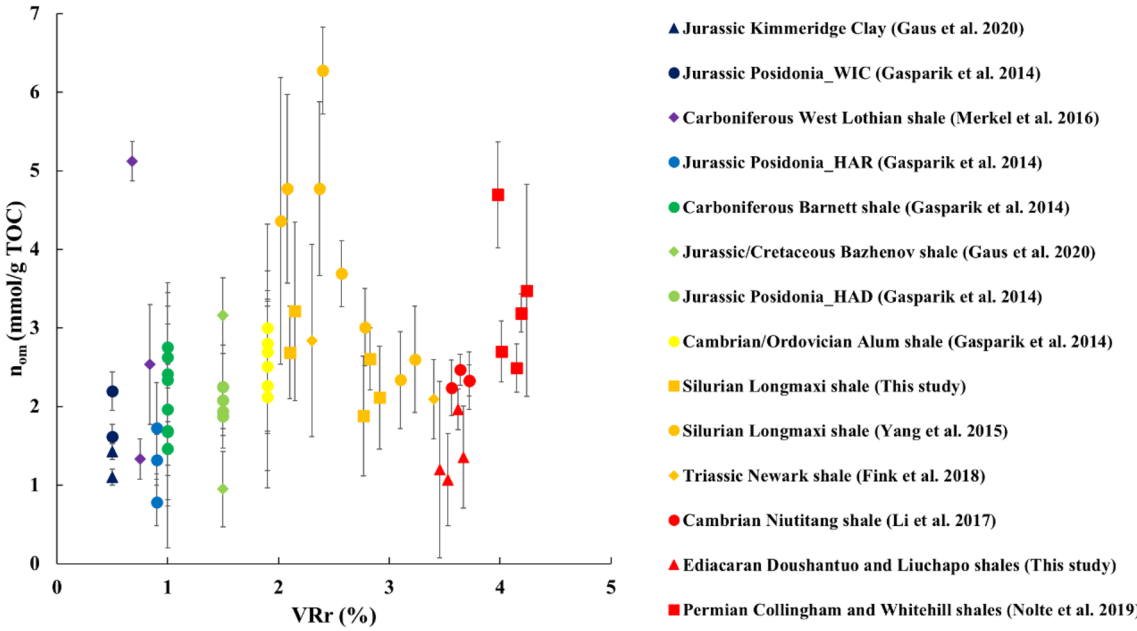

Fig. 12 Relationship of estimated Langmuir volume of organic matter and equivalent vitrinite reflectance (symbols represent estimated Langmuir volumes of organic matter under the assumption of 0.1 mmol/g contribution of clay minerals to total sorption capacity and the error bars reflect assumptions of 0 and 0.2 mmol/g clay mineral contribution)

related to the fact that thermal maturity was strongly influenced by magmatic activity at rather shallow burial depth.

5.3 Pore structure

The strong correlation between TOC content and CO_2 micropore volume and methane sorption capacity indicates that an organic matter associated microporosity mainly controls methane sorption capacity for both samples. However, no correlation was found between TOC content and BET surface area for both shales (Fig. 9a). Considering the relatively high specific surface areas of pure illite (38.5–165.7 m^2/g) (Ziemiański et al. 2020), one possible reason could be that the contribution of clay minerals to the surface area of the studied shales is significant. However, it was shown in chapter 5.1 that clay minerals of the Ediacaran samples do not contribute to the Langmuir volume. According to Gan et al. (1972), Cazorla-Amorós et al. (1998) and Busch et al. (2016), N_2 shows significantly lower diffusivity in micropores smaller than 0.7 nm when compared to CO_2. This phenomenon was also observed in our study, as the CO_2 micropore volumes of two Ediacaran samples and one Silurian sample were significantly higher than the N_2 micropore volumes (Fig. 9c). This resulted in an only partly accessible micropore volume for N_2 at the given experimental conditions. Besides, the interpreted pore size from N_2 adsorption isotherms is between 1.6 and 153 nm, while micropores between 1.2 nm and 1.6 nm can be interpreted from CO_2 isotherms. Therefore, the BET specific surface area derived from N_2 adsorption isotherms could only reflect the apparent specific surface area of relatively coarse micropores, mesopores and fine macropores.

Burial-related compaction in shales leads to a strong reduction of porosity and changes in the pore structure. Vitrinite reflectances of the Ediacaran (VR_r = 3.5–3.7%) and Silurian shales (VR_r = 2.1–3.0%) obtained in this study imply a higher thermal maturity of the Ediacaran shales related to burial. Basin modelling results indicated that maximum burial of the Ediacaran shales likely exceeded a depth of 6000 m whereas burial of the Silurian shales was up to 4500 m (Tan et al. 2013; Zou et al. 2014). This is also reflected by total porosities (Silurian > Ediacaran) and micropore volume fractions (Ediacaran > Silurian) obtained in this study. Pore structures, in addition to burial-related compaction,

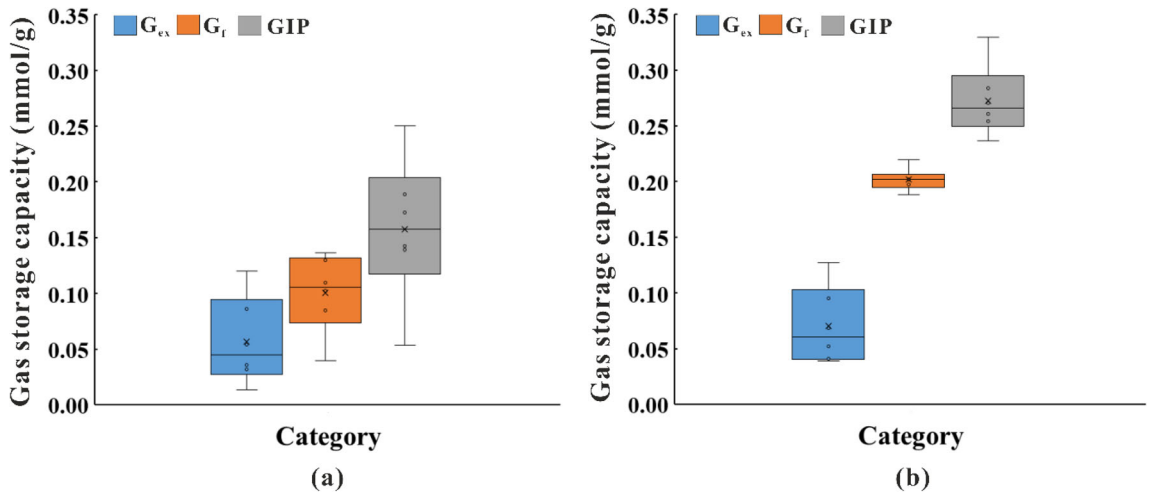

Fig.13 Estimates of excess sorption capacity (G_{ex}), free gas capacity (G_f) and total gas storage capacity (GIP) at a depth of 1200 m and corresponding temperature of 318.15 K for dry Ediacaran (**a**) and Silurian (**b**) shales (average porosity and bulk density of S1, S3 and S5 are used in the calculation of G_f for samples S2, S4 and S6 as porosities of these samples were likely enhanced by weathering)

might also be influenced by the origin of silica. Although XRD measurements from this study revealed similar silica contents for both shales (Table 1), it is likely that the origins of silica in both shales are different (silica biomineralizers are possibly not the main source of silica prior to the Cambrian). Zhao et al. (2017) reported an authigenic microcrystalline quartz content of up to 60% for samples of the Wufeng and Longmaxi formations. This silica content was shown to originate from biogenic silica dissolution and re-crystallization. For Ediacaran rocks it was shown that silica predominantly originated from dissolved silica in oceans (Maliva et al. 1989; Tarhan et al. 2016). Whereas it was shown that biogenic silica ultimately may lead to an increasing rigidity of the rock and therefore to preservation of pore space during burial for the Silurian (Wufeng and Longmaxi) shale (Zhao et al. 2017), it is currently unknown as to how silica derived from non-biogenic sources influenced the pore structure during burial.

A higher micropore volume fraction and lower mesopore volume of the Ediacaran shales when compared to the Silurian shales was observed, which is also reflected by recorded gas uptake data from high-pressure methane sorption experiments (Fig. 5) as equilibration times of the Ediacaran shales are more than two times larger at similar particle sizes (between 63 and 354 µm). Since matrix permeabilities determine the long-term gas production in gas shales (Ghanizadeh et al. 2014; Fink et al. 2018), this observation can be regarded as a first indication of a less favorable pore structure of the Ediacaran shales with respect to long-term production when compared to the Silurian shales.

5.4 Gas-in-place

To estimate the maximum gas-in-place (GIP) quantity, the specific pore volume (free gas) and the excess sorption capacity at reservoir conditions are needed. Based on interpretations of Zhu et al. (2016) and Xu et al. (2018), a geothermal gradient of 25 K/km and a pore pressure gradient of 14.2 MPa/km were used for GIP computations. The average surface temperature was set to 288.15 K. Experimental conditions of the methane sorption isotherms in this study were thus created at reservoir temperatures and covered reservoir pore pressure conditions.

Figure 13 shows free, sorptive and maximum GIP amounts computed for a depth of 1200 m (approximately the current depth of retrieved cores of the Ediacaran samples) for the Ediacaran and Silurian shales at dry conditions. Whereas the computed sorptive storage of the Ediacaran shales (0.014–0.120 mmol/g) is similar to that of the Silurian shales (0.039–0.128 mmol/g), free gas storage amounts are considerably larger for the Silurian shales. Therefore, estimated total gas storage

capacities are lower for the Ediacaran shales (0.054–0.251 mmol/g) when compared to the Silurian shales (0.237–0.330 mmol/g).

Insight into the water saturation of potential shale gas reservoirs is crucial for the accurate assessment of gas reserves as it has a strong control on volumetric and sorptive gas storage. Reported water saturations for the Silurian (Longmaxi) shale range between 20 and 50 vol.% (Hu et al. 2019). No reported water saturations could be found for the Ediacaran shales. Until a critical moisture content is reached, the sorption capacity decreases with increasing amounts of (pre-adsorbed) water (Gasparik et al. 2014; Merkel et al. 2015; Yang et al. 2017). Additional water uptake above this critical moisture content has negligible influence on methane sorption capacity. Yang et al. (2017) reported a 44% to 63% decrease in sorptive methane storage capacity for the Silurian (Longmaxi) shales above the critical moisture content (water content: 1.76 wt.%–4.50 wt.%). Results obtained in this study on two Ediacaran samples show that sorptive methane storage capacities reduce by 32% to 48% above the critical moisture content (water content: 2.14 wt.%–3.08 wt.%). It should therefore be noted that the results from Fig. 13 tend to reflect estimates of maximum gas storage, as these computations do not take account of water saturation and the influence of water vapor on methane sorption capacity.

Previous studies recommended that economically successful shale gas formations exhibit the following characteristics: TOC content $> 2\%$, effective thickness > 30–50 m, brittle mineral content $> 40\%$, porosity $> 2\%$ (Zou et al. 2017; Yasin et al. 2018; Hu et al. 2020a; Yang et al. 2021). Both Ediacaran and Silurian shales are rich in TOC contents (4% in average) and are widely distributed in the Upper Yangtze platform with thicknesses over 100 m. The average brittle mineral contents of both shales exceed 60%, favorable for hydraulic fracturing in shale gas exploitation. The average porosity (3.5%) of Ediacaran shales is approximately half of that (6.8%) in Silurian shales, which leads to lower estimated total gas storage capacities (0.054–0.251 mmol/g) when compared to Silurian shales. However, compared to the gas storage amounts (0.049–0.411 mmol/g) of Fayetteville, Haynesville, Antrim and Marcellus shales from North America, these shales all exceed the lower limit of commercial shale gas development (Zou et al. 2017). High gas production rate achieved from the Ediacaran shale, as mentioned in the introduction, further implies that the oldest potential shale gas formation could be extended from Cambrian to Ediacaran strata. Currently, with respect to Ediacaran shales, only a few studies exist and mainly focus on the pore types, pore size distribution and their relationship with organic matter and minerals (Chen et al. 2016; Yang et al. 2020). Our study also indicates that the pore structure of Ediacaran shales could limit the long-term shale gas production. However, limited by the number and type of Ediacaran samples in this study, experimental permeability measurements on cylindrical specimens could not be performed and thus, evaluations on the relations between the pore network and the matrix permeability should be conducted in a future study.

6 Conclusions

High-pressure CH_4 sorption, low-pressure N_2 / CO_2 adsorption and water immersion porosimetry measurements were performed on Ediacaran (Liuchapo and Doushantuo formations) and Lower Silurian (Longmaxi formation) shales from the Upper Yangtze platform to characterize and compare pore structures as well as maximum methane storage capacities. The following conclusions can be drawn:

(1) Maximum sorption capacities (Langmuir volumes) of Ediacaran and Silurian shales at dry conditions ranged between 0.02–0.19 mmol/g and 0.08–0.21 mmol/g, respectively. TOC content exhibits significant control on sorption capacity and CO_2 micropore volume shows a strong positive correlation with TOC content for both shales. Clay types but more importantly evolutionary differences during burial and different origins of illite could affect the sorptive storage. Additionally, a strong negative impact of water on methane sorption capacity of up to 64% (comparison of excess sorption at 10 MPa of samples in dry and moisturized state) was observed for the Ediacaran shales.

(2) Computed total gas storage capacities (sorptive and free gas amounts combined) at present day reservoir conditions are lower for the Ediacaran shales (0.054–0.251 mmol/g) when compared to the Silurian shales (0.237–0.330 mmol/g).
(3) Total porosities (Silurian > Ediacaran), mesopore volumes (Silurian > Ediacaran) and micropore volume fractions (Ediacaran > Silurian) indicate that compaction had a stronger influence on the Ediacaran shale. This could be related to deeper burial (larger vitrinite reflectances for the Ediacaran shales) but also to the origin of silica (biogenic vs. abiogenic) as silica biomineralizers were likely not the main source of silica prior to the Cambrian. A lower diffusion efficiency of the Ediacaran shales when compared to the Silurian shales was observed from gas uptake data of high-pressure methane sorption experiments. This observation can be regarded as a first indication of a less favorable pore structure of the Ediacaran shales with respect to long-term production when compared to the Silurian shales.
(4) The influence of thermal maturity on maximum methane sorption capacities of organic matter was investigated by comparison of shales with vitrinite reflectances ranging from 0.5 to 4.24% and TOC contents ranging from 2.2 to 45.0 wt.%. A clear relationship of maximum sorption capacity of organic matter and thermal maturity could not be identified as combined variations of sorption capacity due to sample preparation (particle size), sample heterogeneity, burial history and most importantly false estimations of clay mineral contribution to overall sorption capacity are larger than potential trends due to thermal maturity.

Acknowledgements Financial support from China Scholarship Council is highly acknowledged. We are also thankful for the technical support from Patrick Thelen during conduction of the sorption measurements.

Funding Open Access funding enabled and organized by Projekt DEAL.

Declarations

Conflict of interest The authors declare that they have no known competing financial interests or personal relationships that could have appeared to influence the work reported in this paper.

Appendix 1

See Fig. 14.

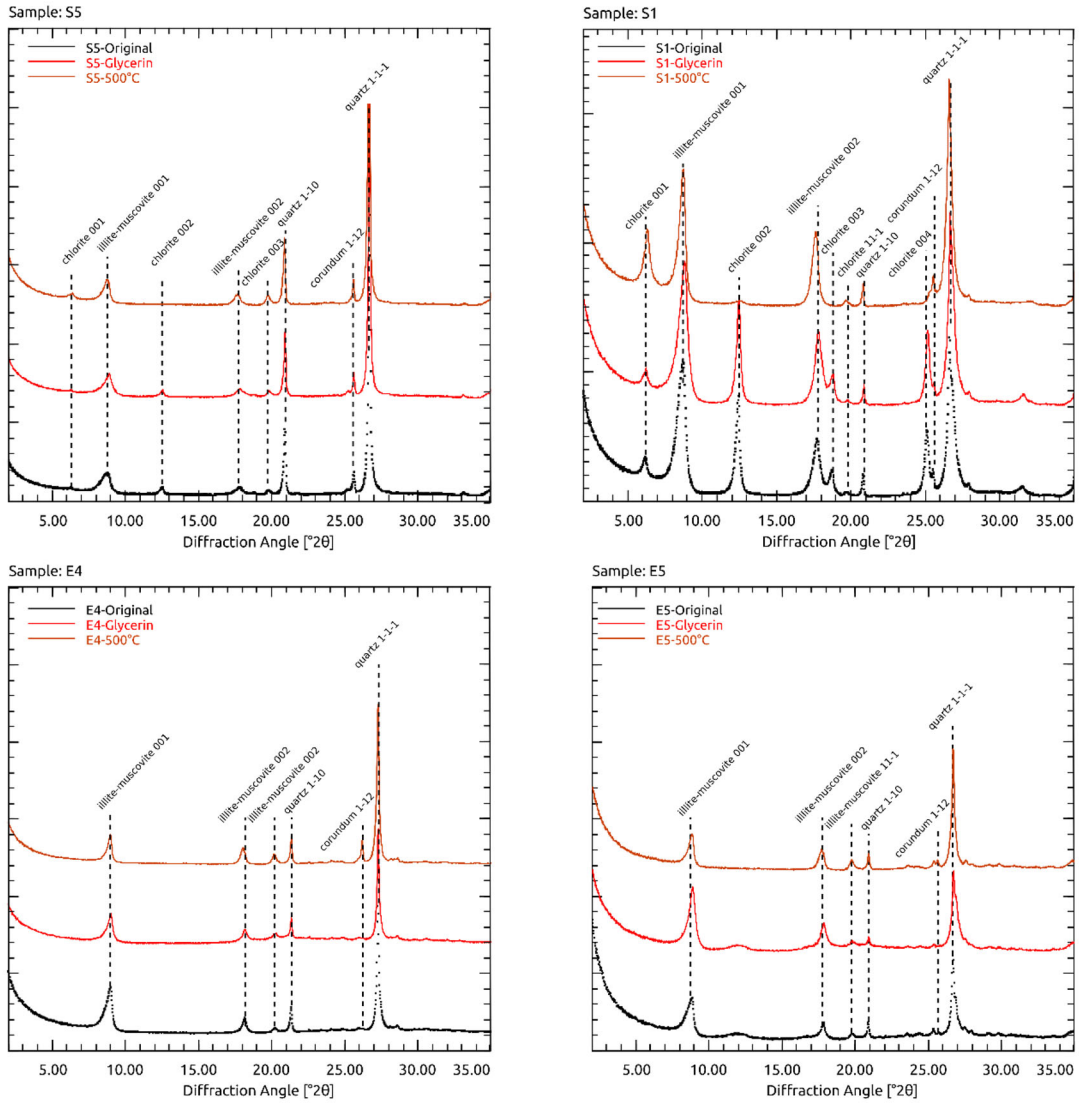

Fig. 14 X-ray diffraction pattern of separated clay fraction measured as texture preparations of four representative shale samples (S5, S1, E4, E5); representing the untreated, original sample (black), the glycerin treated sample (red) and heated sample (orange). Reflections are labeled according to the individual mineral and its corresponding hkl's

References

Barrett EP, Joyner LG, Halenda PP (1951) The Determination of pore volume and area distributions in porous substances. I. Computations from nitrogen isotherms. J Am Chem Soc 73:373–380. https://doi.org/10.1021/ja01145a126

Berner RA, Raiswell R (1984) C/S method for distinguishing freshwater from marine sedimentary rocks. Geology 12:365–368. https://doi.org/10.1130/0091-7613(1984)12%3c365:CMFDFF%3e2.0.CO;2

Brunauer S, Emmett PH, Teller E (1938) Adsorption of gases in multimolecular layers. J Am Chem Soc 60:309–319. https://doi.org/10.1021/ja01269a023

Busch A, Bertier P, Gensterblum Y, Rother G, Spiers CJ, Zhang M, Wentinck HM (2016) On sorption and swelling of CO_2 in clays. Geomech Geophys Geo-Energ Geo-Resour 2:111–130. https://doi.org/10.1007/s40948-016-0024-4

Cazorla-Amoros D, Alcaniz-Monge J, de la Casa-Lillo MA, Linares-Solano A (1998) CO_2 as an adsorptive to characterize carbon molecular sieves and activated carbons. Langmuir 14:4589–4596. https://doi.org/10.1021/la980198p

Chalmers GRL, Bustin RM (2007) The organic matter distribution and methane capacity of the lower Cretaceous strata of northeastern British Columbia, Canada. Int J Coal Geol 70:223–239. https://doi.org/10.1016/j.coal.2006.05.001

Charvet J (2013) The Neoproterozoic-Early Paleozoic tectonic evolution of the South China Block: an overview. J Asian Earth Sci 74:198–209. https://doi.org/10.1016/j.jseaes.2013.02.015

Chen JH (2018) Shale gas exploration and development progress in china and the way forward. IOP Conference Series: Earth and Environmental Science. https://doi.org/10.1088/1755-1315/113/1/012178

Chen Q, Zhang JC, Tang X, Li WJ, Li ZM (2016) Relationship between pore type and pore size of marine shale: An example from the Sinian-Cambrian formation, upper Yangtze region, South China. Int J Coal Geol 158:13–28. https://doi.org/10.1016/j.coal.2016.03.001

Clarkson CR et al (2016) Nanopores to megafractures: Current challenges and methods for shale gas reservoir and hydraulic fracture characterization. J Nat Gas Sci Eng 31:612–657. https://doi.org/10.1016/j.jngse.2016.01.041

Clarkson CR, Bustin RM (1996) Variation in micropore capacity and size distribution with composition in bituminous coal of the Western Canadian Sedimentary Basin - Implications for coalbed methane potential. Fuel 75:1483–1498. https://doi.org/10.1016/0016-2361(96)00142-1

Dai J, Dong D, Ni Y, Hong F, Zhang S, Zhang Y, Ding L (2020) Some essential geological and geochemical issues about shale gas research in China. Nat Gas Geosci 31:745–760

Dang W, Zhang J, Tang X, Chen Q, Han S, Li Z, Du X, Wei X, Zhang M, Liu J, Peng J (2016) Shale gas potential of Lower Permian marine-continental transitional black shales in the Southern North China Basin, central China: Characterization of organic geochemistry. J Nat Gas Sci Eng 28:639–650. https://doi.org/10.1016/j.jngse.2015.12.035

Deng B, Liu SG, Liu S, Li ZW, Zhao JC (2009) Restoration of exhumation thickness and its significance in Sichuan Basin. J Chengdu Univ Technol Sci Technol Ed 36:675–686

Doebelin N, Kleeberg R (2015) Profex: a graphical user interface for the Rietveld refinement program BGMN. J Appl Crystallogr 48:1573–1580. https://doi.org/10.1107/S1600576715014685

Dreisbach F, Staudt R, Keller JU (1999) High pressure adsorption data of methane, nitrogen, carbon dioxide and their binary and ternary mixtures on activated carbon. Adsorption 5:215–227. https://doi.org/10.1023/A:1008914703884

Dubinin MM, Astakhov VA (1971) Development of the concepts of volume filling of micropores in the adsorption of gases and vapors by microporous adsorbents. Bull Acad Sci USSR Div Chem Sci 20:8–12

Fink R, Amann-Hildenbrand A, Bertier P, Littke R (2018) Pore structure, gas storage and matrix transport characteristics of lacustrine Newark shale. Mar Petrol Geol 97:525–539. https://doi.org/10.1016/j.marpetgeo.2018.06.035

Gan H, Nandi SP, Walker PL Jr (1972) Nature of the porosity in American coals. Fuel 51:272–277. https://doi.org/10.1016/0016-2361(72)90003-8

Gasparik M, Bertier P, Gensterblum Y, Ghanizadeh A, Krooss BM, Littke R (2014) Geological controls on the methane storage capacity in organic-rich shales. Int J Coal Geol 123:34–51. https://doi.org/10.1016/j.coal.2013.06.010

Gaus G, Fink R, Amann-Hildenbrand A, Krooss BM, Littke R (2021) Experimental determination of porosity and methane sorption capacity of organic-rich shales as a function of effective stress: Implications for gas storage capacity. AAPG Bull 105:309–328. https://doi.org/10.1306/07212019086

Gaus G, Kalmykov A, Krooss BM, Fink R (2020) Experimental investigation of the dependence of accessible porosity and methane sorption capacity of carbonaceous shales on particle size. Geofluids. https://doi.org/10.1155/2020/2382153

Gensterblum Y et al (2009) European inter-laboratory comparison of high pressure CO_2 sorption isotherms. I: Activated carbon. Carbon 47:2958–2969. https://doi.org/10.1016/j.carbon.2009.06.046

Ghanizadeh A, Gasparik M, Amann-Hildenbrand A, Gensterblum Y, Krooss BM (2014) Experimental study of fluid transport processes in the matrix system of the European organic-rich shales: I. Scand Alum Shale Mar Petrol Geol 51:79–99. https://doi.org/10.1016/j.marpetgeo.2013.10.013

Guo QJ et al (2007) Trace element chemostratigraphy of two Ediacaran-Cambrian successions in South China: Implications for organosedimentary metal enrichment and silicification in the early Cambrian. Palaeogeogr Palaeocl 254:194–216. https://doi.org/10.1016/j.palaeo.2007.03.016

Gurvich LG (1915) Acerca de la fuerza de atraccio´n fisicoqui´mica [On the physico-chemical force of attraction]. J Phys Chem Soc Russia 47:805–827

Han SB, Zhang JC, Li YX, Horsfield B, Tang X, Jiang WL, Chen Q (2013) Evaluation of lower cambrian shale in Northern Guizhou Province, South China: implications for shale gas potential. Energ Fuel 27:2933–2941. https://doi.org/10.1021/ef400141m

Hantschel TH, Kauerauf A (2009) Fundamentals of basin and petroleum system modeling. Springer. https://doi.org/10.1007/978-3-540-72318-9

Hildenbrand A, Krooss BM, Busch A, Gaschnitz R (2006) Evolution of methane sorption capacity of coal seams as a function of burial history—a case study from the Campine Basin, NE Belgium. Int J Coal Geol 66:179–203. https://doi.org/10.1016/j.coal.2005.07.006

Hu HY, Zhang TW, Wiggins-Camacho JD, Ellis GS, Lewan MD, Zhang XL (2015) Experimental investigation of changes in methane adsorption of bitumen-free Woodford Shale with thermal maturation induced by hydrous pyrolysis. Mar Petrol Geol 59:114–128. https://doi.org/10.1016/j.marpetgeo.2014.07.029

Hu Y, Li X, Zhang Z, He J, Li G (2020a) Numerical investigation on the hydraulic stimulation of naturally fractured Longmaxi shale reservoirs using an extended discontinuous deformation analysis (DDA) method. Geomech Geophys Geo-Energ Geo-Resour 6:1–21. https://doi.org/10.1007/s40948-020-00195-5

Hu Z, Duan X, He Y, Wu J, Chang J, Liu L, Wu K, Ma Z (2019) Influence of reservoir primary water on shale gas occurrence and flow capacity. Nat Gas Ind. https://doi.org/10.1016/j.ngib.2019.01.010

Hu ZZ, Klaver J, Schmatz J, Dewanckele J, Littke R, Krooss BM, Amann-Hildenbrand A (2020b) Stress sensitivity of

porosity and permeability of Cobourg limestone. Eng Geol. https://doi.org/10.1016/j.enggeo.2020.105632

Ji LM, Zhang TW, Milliken KL, Qu JL, Zhang XL (2012) Experimental investigation of main controls to methane adsorption in clay-rich rocks. Appl Geochem 27:2533–2545. https://doi.org/10.1016/j.apgeochem.2012.08.027

Klaver J, Desbois G, Littke R, Urai JL (2015) BIB-SEM characterization of pore space morphology and distribution in postmature to overmature samples from the Haynesville and Bossier Shales. Mar Petrol Geol 59:451–466. https://doi.org/10.1016/j.marpetgeo.2014.09.020

Krooss BM, van Bergen F, Gensterblum Y, Siemons N, Pagnier HJM, David P (2002) High-pressure methane and carbon dioxide adsorption on dry and moisture-equilibrated Pennsylvanian coals. Int J Coal Geol 51:69–92. https://doi.org/10.1016/S0166-5162(02)00078-2

Kuila U, McCarty DK, Derkowski A, Fischer TB, Prasad M (2014) Total porosity measurement in gas shales by the water immersion porosimetry (WIP) method. Fuel 117:1115–1129. https://doi.org/10.1016/j.fuel.2013.09.073

Kunz O, Wagner W (2012) The GERG-2008 Wide-Range Equation of State for Natural Gases and Other Mixtures: An Expansion of GERG-2004. J Chem Eng Data 57:3032–3091. https://doi.org/10.1021/je300655b

Li HH, Chen K, Bao SJ, Zhang YL, Song T, Wang P (2019) Evaluation of shale gas resources of the Sinian Doushantuo Formation in the southern Huangling anticline, western Hubei Province. Pet Geol Exp 41:31–37

Li P, Zhang JC, Tang X, Huo ZP, Li Z, Luo KY, Li ZM (2020) Assessment of shale gas potential of the lower Permian transitional Shanxi-Taiyuan shales in the southern North China Basin. Aust J Earth Sci. https://doi.org/10.1080/08120099.2020.1762737

Li TF, Tian H, Xiao XM, Cheng P, Zhou Q, Wei Q (2017) Geochemical characterization and methane adsorption capacity of overmature organic-rich Lower Cambrian shales in northeast Guizhou region, southwest China. Mar Petrol Geol 86:858–873. https://doi.org/10.1016/j.marpetgeo.2017.06.043

Liang LX, Xiong J, Liu XJ, Luo DX (2016) An investigation into the thermodynamic characteristics of methane adsorption on different clay minerals. J Nat Gas Sci Eng 33:1046–1055. https://doi.org/10.1016/j.jngse.2016.06.024

Littke R, Klussmann U, Krooss B, Leythaeuser D (1991) Quantification of loss of calcite, pyrite, and organic-matter due to weathering of toarcian black shales and effects on kerogen and bitumen characteristics. Geochim Cosmochim Ac 55:3369–3378. https://doi.org/10.1016/0016-7037(91)90494-P

Littke R, Urai JL, Uffmann AK, Risvanis F (2012) Reflectance of dispersed vitrinite in Palaeozoic rocks with and without cleavage: Implications for burial and thermal history modeling in the Devonian of Rursee area, northern Rhenish Massif, Germany. Int J Coal Geol 89:41–50. https://doi.org/10.1016/j.coal.2011.07.006

Lu XC, Li FC, Watson AT (1995) Adsorption measurements in Devonian shales. Fuel 74:599–603. https://doi.org/10.1016/0016-2361(95)98364-K

Mählmann RF, Frey M (2012) Standardisation, calibration and correlation of the Kubler-index and the vitrinite/bituminite reflectance: an inter-laboratory and field related study. Swiss J Geosci 105:153–170. https://doi.org/10.1007/s00015-012-0110-8

Maliva RG, Knoll AH, Siever R (1989) Secular Change in chert distribution: a reflection of evolving biological participation in the silica cycle. Palaios 4:519–532. https://doi.org/10.2307/3514743

Mcdowell SD, Elders WA (1980) Authigenic layer silicate minerals in borehole elmore-1, salton-sea geothermal-field, California, USA. Contrib Mineral Petr 74:293–310. https://doi.org/10.1007/Bf00371699

Merkel A, Fink R, Littke R (2015) The role of pre-adsorbed water on methane sorption capacity of Bossier and Haynesville shales. Int J Coal Geol 147:1–8. https://doi.org/10.1016/j.coal.2015.06.003

Merkel A, Fink R, Littke R (2016) High pressure methane sorption characteristics of lacustrine shales from the Midland Valley Basin, Scotland. Fuel 182:361–372. https://doi.org/10.1016/j.fuel.2016.05.118

Mikutta R, Kleber M, Kaiser K, Jahn R (2005) Review: Organic matter removal from soils using hydrogen peroxide, sodium hypochlorite, and disodium peroxodisulfate. Soil Sci Soc Am J 69:120–135. https://doi.org/10.2136/sssaj2005.0120

Nie HK, Tang X, Bian RK (2009) Controlling factors for shale gas accumulation and prediction of potential development area in shale gas reservoir of South China. Acta Petrolei Sinica 30:484–491

Nolte S, Geel C, Amann-Hildenbrand A, Krooss BM, Littke R (2019) Petrophysical and geochemical characterization of potential unconventional gas shale reservoirs in the southern Karoo Basin. South Africa Int J Coal Geol. https://doi.org/10.1016/j.coal.2019.103249

Ren JS, Niu BG, Wang J, Jin XC, Zhao L, Liu RY (2013) Advances in research of Asian geology-A summary of 1:5M International Geological Map of Asia project. J Asian Earth Sci 72:3–11. https://doi.org/10.1016/j.jseaes.2013.02.006

Rexer TF, Mathia EJ, Aplin AC, Thomas KM (2014) High-pressure methane adsorption and characterization of pores in posidonia shales and isolated kerogens. Energ Fuel 28:2886–2901. https://doi.org/10.1021/ef402466m

Rexer TFT, Benham MJ, Aplin AC, Thomas KM (2013) Methane adsorption on shale under simulated geological temperature and pressure conditions. Energ Fuel 27:3099–3109. https://doi.org/10.1021/ef400381v

Ross DJK, Bustin RM (2009) The importance of shale composition and pore structure upon gas storage potential of shale gas reservoirs. Mar Petrol Geol 26:916–927. https://doi.org/10.1016/j.marpetgeo.2008.06.004

Rouquerol J, Rouquerol F, Llewellyn P, Maurin G, Sing KSW (2013) Adsorption by powders and porous solids: principles. Elsevier, Methodology and Applications

Seemann T, Bertier P, Krooss B, Stanjek H (2017) Water vapour sorption on mudrocks. Geological Society, London, Special Publications. https://doi.org/10.1144/SP454.8

Tan JQ, Horsfield B, Mahlstedt N, Zhang J, di Primio R, Vu TA, Boreham CJ, van Graas G, Tocher BA (2013) Physical properties of petroleum formed during maturation of

Lower Cambrian shale in the upper Yangtze Platform, South China, as inferred from PhaseKinetics modelling. Mar Petrol Geol 48:47–56. https://doi.org/10.1016/j.marpetgeo.2013.07.013

Tarhan LG, Hood AVS, Droser ML, Gehling JG, Briggs DEG (2016) Exceptional preservation of soft-bodied Ediacara Biota promoted by silica-rich oceans. Geology 44:951–954. https://doi.org/10.1130/G38542.1

Taylor GH, Teichmüller M, Glick DC, Davis A (1998) Organic Petrology: A New Handbook Incorporating Some Revised Parts of Stach's Textbook of Coal Petrology. Gebrüder Borntraeger

Thommes M, Kaneko K, Neimark AV, Olivier JP, Rodriguez-Reinoso F, Rouquerol J, Sing KS (2015) Physisorption of gases, with special reference to the evaluation of surface area and pore size distribution (IUPAC Technical Report). Pure Appl Chem 87(9–10):1051–1069. https://doi.org/10.1515/pac-2014-1117

Ufer K, Kleeberg R (2015) Parametric Rietveld refinement of coexisting disordered clay minerals. Clay Miner 50:287–296. https://doi.org/10.1180/claymin.2015.050.3.03

Ufer K, Stanjek H, Roth G, Dohrmann R, Kleeberg R, Kaufhold S (2008) Quantitative phase analysis of bentonites by the Rietveld method. Clay Clay Miner 56:272–282. https://doi.org/10.1346/Ccmn.2008.0560210

Uffmann AK, Littke R, Rippen D (2012) Mineralogy and geochemistry of Mississippian and Lower Pennsylvanian Black Shales at the Northern Margin of the Variscan Mountain Belt (Germany and Belgium). Int J Coal Geol 103:92–108. https://doi.org/10.1016/j.coal.2012.08.001

Vandenbroucke M, Largeau C (2007) Kerogen origin, evolution and structure. Org Geochem 38:719–833. https://doi.org/10.1016/j.orggeochem.2007.01.001

Waliczek M, Machowski G, Poprawa P, Świerczewska A, Więcław D (2021) A novel VR_o, T_{max}, and S indices conversion formulae on data from the fold-and-thrust belt of the Western Outer Carpathians (Poland). Int J Coal Geol 234:103672. https://doi.org/10.1016/j.coal.2020.103672

Wang PF, Jiang Z, Chen L, Yin L, Li Z, Zhang C, Tang X, Wang G (2016) Pore structure characterization for the Longmaxi and Niutitang shales in the Upper Yangtze Platform, South China: Evidence from focused ion beam He ion microscopy, nano-computerized tomography and gas adsorption analysis. Mar Petrol Geol 77:1323–1337. https://doi.org/10.1016/j.marpetgeo.2016.09.001

Wang YF, Zhai GY, Lu YC, Ma YQ, Li J, Liu GH, Zhang YX (2019) Sedimentary lithofacies characteristics and sweet-spot interval characterization of the Sinian Doushantuo Formation in Upper Yangtze Platform, South China. China Geol 2:261–275. https://doi.org/10.31035/cg2018119

Wang ZG, Tan XC (1994) Palaeozoic structural evolution of Yunnan. J SE Asian Earth Sci 9:345–348. https://doi.org/10.1016/0743-9547(94)90045-0

Weaver CE (1967) Potassium Illite and Ocean. Geochim Cosmochim Ac 31:2181–2196. https://doi.org/10.1016/0016-7037(67)90060-9

Weaver CE (1989) Clays, Muds, and Shales. Elsevier

Wu SJ, Wei GQ, Yang W, Xie WR, Zeng FY (2016) Tongwan Movement and its geologic significances in Sichuan Basin. Nat Gas Geosci 27:60–70. https://doi.org/10.11764/j.issn.1672-1926.2016.01.0060

Xu H, Zhou W, Cao Q, Xiao C, Zhou QM, Zhang HT, Zhang YY (2018) Differential fluid migration behaviour and tectonic movement in Lower Silurian and Lower Cambrian shale gas systems in China using isotope geochemistry. Mar Petrol Geol 89:47–57. https://doi.org/10.1016/j.marpetgeo.2017.03.027

Yang B, Xue L, Duan Y, Wang M (2021) Correlation study between fracability and brittleness of shale-gas reservoir. Geomech Geophys Geo-Energ Geo-Resour 7:1–3. https://doi.org/10.1007/s40948-021-00231-y

Yang F, Ning ZF, Zhang R, Zhao HW, Krooss BM (2015) Investigations on the methane sorption capacity of marine shales from Sichuan Basin, China. Int J Coal Geol 146:104–117. https://doi.org/10.1016/j.coal.2015.05.009

Yang F, Xie CJ, Ning ZF, Krooss BM (2017) High-Pressure methane sorption on dry and moisture-equilibrated shales. Energ Fuel 31:482–492. https://doi.org/10.1021/acs.energyfuels.6b02999

Yang R, He S, Hu QH, Hu DF, Zhang SW, Yi JZ (2016) Pore characterization and methane sorption capacity of over-mature organic-rich Wufeng and Longmaxi shales in the southeast Sichuan Basin, China. Mar Petrol Geol 77:247–261. https://doi.org/10.1016/j.marpetgeo.2016.06.001

Yang W, He S, Zhai G, Tao Z, Dong T, Han Y, Chen K, Wei S (2020) Pore characteristics of the lower Sinian Doushantuo Shale in the Mid-Yangtze Yichang area of China: Insights into a distinct shale gas reservoir in the Neoproterozoic formation. J Nat Gas Sci Eng. https://doi.org/10.1016/j.jngse.2019.103085

Yasin Q, Du Q, Sohail GM, Ismail A (2018) Fracturing index-based brittleness prediction from geophysical logging data: application to Longmaxi shale. Geomech Geophys Geo-Energ Geo-Resour 4:301–325. https://doi.org/10.1007/s40948-018-0088-4

Yuan Y, Sun D, Li S, Lin J (2013) Caledonian erosion thickness reconstruction in the Sichuan Basin. Sci Geol Sin 48:581–591. https://doi.org/10.3969/j.issn.0563-5020.2013.03.001

Zhai GM (1987) Petroleum geology of China. vol 10. Petroleum Industry Press

Zhai GY, Wang YF, Zhou Z, Liu GH, Yang YR, Li J (2018) "Source-Diagenesis-Accumulation" enrichment and accumulation regularity of marine shale gas in southern China. China Geol 1:319–330. https://doi.org/10.31035/cg2018059

Zhang Q, Littke R, Zieger L, Shabani M, Tang X, Zhang JC (2019) Ediacaran, Cambrian, Ordovician, Silurian and Permian shales of the Upper Yangtze Platform, South China: Deposition, thermal maturity and shale gas potential. Int J Coal Geol. https://doi.org/10.1016/j.coal.2019.103281

Zhang TW, Ellis GS, Ruppel SC, Milliken K, Yang RS (2012) Effect of organic-matter type and thermal maturity on methane adsorption in shale-gas systems. Org Geochem 47:120–131. https://doi.org/10.1016/j.orggeochem.2012.03.012

Zhao JH, Jin ZK, Jin ZJ, Wen X, Geng YK (2017) Origin of authigenic quartz in organic-rich shales of the Wufeng and

Longmaxi Formations in the Sichuan Basin, South China: Implications for pore evolution. J Nat Gas Sci Eng 38:21–38. https://doi.org/10.1016/j.jngse.2016.11.037

Zhu CQ, Hu SB, Qiu NS, Rao S, Yuan YS (2016) The thermal history of the Sichuan Basin, SW China: Evidence from the deep boreholes. Sci China Earth Sci 59:70–82. https://doi.org/10.1007/s11430-015-5116-4

Ziemiański PP, Derkowski A, Szczurowski J, Koziel M (2020) The structural versus textural control on the methane sorption capacity of clay minerals. Int J Coal Geol. https://doi.org/10.1016/j.coal.2020.103483

Zou CN (2017) Unconventional petroleum geology. Elsevier, Boston, MA

Zou CN et al (2014) Formation, distribution, resource potential, and discovery of Sinian-Cambrian giant gas field, Sichuan Basin, SW China. Petrol Explor Dev 41:306–325. https://doi.org/10.1016/S1876-3804(14)60036-7

Zou CN et al (2016) Shale gas in China: Characteristics, challenges and prospects (II). Petrol Explor Dev 43:182–196. https://doi.org/10.1016/S1876-3804(16)30022-2